DOI: 10.1002/cmdc.200700198

A Multidisciplinary Approach for the Identification of Novel HIV-1 Non-Nucleoside Reverse Transcriptase Inhibitors: S-DABOCs and DAVPs

Marco Radi,[a] Chiara Falciani,[a] Lorenzo Contemori,[a] Elena Petricci,[a] Giovanni Maga,[b] Alberta Samuele,[b] Samantha Zanoli,[b] Montserrat Terrazas,[c] Marinunzia Castria,[a] Andrea Togninelli,[a] José A. Esté,[d] Imma Clotet-Codina,[d] Mercedes Armand-Ugón,[d] and Maurizio Botta*[a]

Dedicated to Paolo Malizia for support in the earlier times of his career.

Among the FDA approved drugs for the treatment of AIDS, non-nucleoside reverse transcriptase inhibitors (NNRTIs) are essential components of first-line anti-HIV-1 therapy because of the less-severe adverse effects associated with NNRTIs administration in comparison to therapies based on other anti-HIV-1 agents. In this contest, 3,4-dihydro-2-alkoxy-6-benzyl-4-oxypyrimidines (DABOs) have been the object of many studies aimed at identifying novel analogues endowed with potent inhibitory activity towards HIV-1 wild type and especially drug-resistant mutants. Accordingly, based on the encouraging results obtained from the biological screening of our internal collection of S-DABO derivatives, we started with the systematic functionalization of the pyrimidine scaffold to identify the minimal required structural features for RT inhibition. Herein, we describe how the combination of synthetic, biological, and molecular modeling studies led to the identification of two novel subclasses of S-DABO analogues: S-DABO cytosine analogues (S-DABOCs) and 4-dimethyamino-6-vinylpyrimidines (DAVPs).

Introduction

The acquired immunodeficiency syndrome (AIDS) related to HIV-1 infection is one of the most serious threats to human health, with an estimated number of people living with the virus now passing 45 million worldwide (world health organization web report on the global HIV/AIDS epidemic, 2005).[1] Important advances in the AIDS treatment have been made with the discovery of new drugs and the administration of "cocktails" of drugs targeting the viral enzymes reverse transcriptase (RT) and protease (PR), a treatment strategy known as HAART (highly active antiretroviral therapy). Among the FDA approved drugs for the treatment of AIDS, first and second generation non-nucleoside reverse transcriptase inhibitors (NNRTIs) are essential components of first-line anti-HIV-1 therapy because of their good tolerability and no association with lipodystrophy which generally accompanies the administration of protease inhibitors.[2] However, the efficacy of currently available NNRTIs, for example, nevirapine (NVP, Viramune), delavirdine (DLV, Rescriptor), and efavirenz (EFV, Sustiva, Stocrin), is impaired by rapid emergence of drug resistance. Consequently, as patients live longer on HAART therapy and the pool of NNRTI-resistant viruses increases, so does the need for the development of new drugs with antiviral activity against clinically relevant mutant strains. NNRTIs include more then 30 structurally different classes of molecules, such as nevirapine, TIBO, HEPT, TNK-561, ITU, DATA, and DAPY.[3] These compounds bind to a specific allosteric site of HIV-1 RT near the polymerase active site and interfere with reverse transcription by altering either the conformation or mobility of RT thereby leading to a noncompetitive inhibition of the enzyme. Among the NNRTIs reported to date, 3,4-dihydro-2-alkoxy-6-benzyl-4-oxypyrimidines (DABOs) have been the object of many studies aimed at identifying novel analogues endowed with potent inhibitory activity towards HIV-1 wild type and especially drug resistant mutants. Since 1992, when the first DABO analogue was identified[4] (compound **1** Figure 1), a number of functionalizations have been introduced at the 4(3*H*)-pyrimidinone scaffold leading to highly functionalized S-DABOs, NH-DABOs, and DATNOs derivatives.[5] However, although the 4-amino analogue **2** (Figure 1) identified in 1992[4] had a stronger anti-HIV-1 activity in com-

[a] *Dr. M. Radi, Dr. C. Falciani, Dr. L. Contemori, Dr. E. Petricci, Dr. M. Castria, Dr. A. Togninelli, Prof. M. Botta*
Dipartimento Farmaco Chimico Tecnologico, University of Siena
Via Alcide de Gasperi 2, 53100 Siena (Italy)
Fax: (+39) 0577-234333
E-mail: botta@unisi.it

[b] *Dr. G. Maga, Dr. A. Samuele, Dr. S. Zanoli*
Istituto di Genetica Molecolare, IGM-CNR
Via Abbiategrasso 207, 27100 Pavia (Italy)

[c] *Dr. M. Terrazas*
Departament de Química Orgànica
Facultat de Química, Universitat de Barcelona
Av. Diagonal 647, 08028 Barcelona (Spain)

[d] *Prof. J. A. Esté, Dr. I. Clotet-Codina, Dr. M. Armand-Ugón*
Retrovirology Laboratory irsiCaixa
Hospital Universitari Germans Trias i Pujol
Universitat Autonoma de Barcelona, 08916 Badalona (Spain)

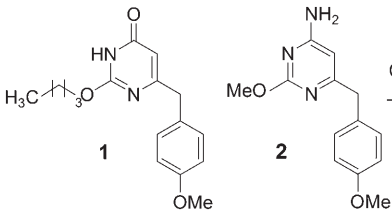

Compd.	HV-1 ED_{90} (μg/mL)	HV-1 TD_{50} (μg/mL)
1	25	100
2	12.5	50

Figure 1. The first identified DABO (**1**) and its 4-amino analogue **2**.

parison with its DABO precursor **1**, poor or little attention was paid to these cytosine derivatives.

The present paper summarize our recent efforts for the discovery of novel NNRTIs. It will been shown how the combination of synthetic, biological, and molecular modeling studies led to the identification of two novel and promising classes of NNRTIs, namely 1) S-DABO cytosine analogues (S-DABOCs) possessing interesting activity towards NNRTIs resistant mutants and 2) 4-dimethylamino-6-vinylpyrimidines (DAVPs) representing the first NNRTIs competing with the nucleotide substrate after binding to the non-nucleoside inhibitors binding pocket (NNIBP) of the free enzyme.

NNRTIs and RT mutations

Structural and biochemical data reveal that, albeit structurally very different, first and second generation NNRTIs bind to a hydrophobic pocket (the non-nucleoside inhibitor binding pocket, NNIBP) situated in the p66 subunit of the heterodimeric enzyme, about 10 Å away from the active site.[6–9] Comparison of the unliganded RT structure with those of RT–NNRTIs complexes shows that, in the inhibitor-free structure, there is a small solvent inaccessible cavity between Y181, Y183, and Y188. Upon inhibitor binding, these three residues rotate "outwards", filling this cavity and opening a large solvent-accessible cavity (600–700 Å) lined by a number of hydrophobic residues, where NNRTIs binding occurs. This movement restricts the flexibility and mobility of the thumb domain and locks it in an open conformation.[10,11] Whereas first-generation NNRTIs adopt an almost rigid butterfly-like conformation within the binding site,[12] second-generation NNRTIs are more flexible and show additional contacts with the amino acid residues of the NNIBP.[13] The ability to make contacts with residues that are unlikely to be disrupted by single mutations may explain the ability of second-generation NNRTIs to retain activity in the presence of mutations conferring resistance to first generation NNRTIs. The first RT mutations shown to be associated with resistance to NNRTIs were K103N and Y181C, which were selected in the presence of pyridinone derivatives such as nevirapine (NVP) and TIBO R82150. Indeed, the K103N and Y181C mutations have been observed with virtually all currently available NNRTIs.[14,15] Other drug-specific mutations include L100I, V106A, and P236L. All the amino acids mutated in the NNIBP reduce the number of stabilizing interactions with the drug. One noteworthy exception is the mutation K103N, which lines the proposed entry channel for the NNRTIs. Enzymological and crystallographic studies showed that this mutation imposes a thermodynamic barrier for the formation of the RT–inhibitor complex, most likely by creating a hydrogen bond not present in the wild-type enzyme.[15] It has therefore been proposed that the K103N mutation determines a novel mechanism of drug resistance by stabilizing the closed form of the NNIBP, thus slowing down the association rate of the enzyme to the NNRTIs.[16]

Designing simplified S-DABO analogues

Recently, biological screening of our internal S-DABO collection[17] allowed identification compound **3** as a potent inhibitor of HIV-1 RT (Figure 2). Molecular docking simulations, showed

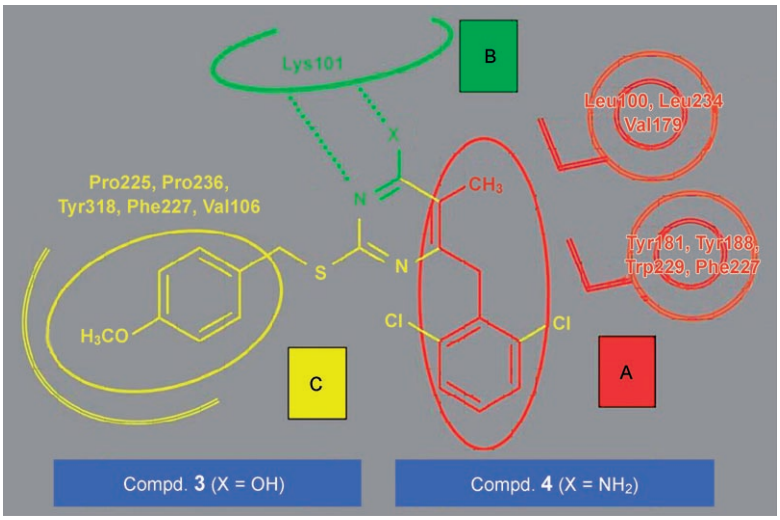

Figure 2. Key interactions of S-DABO **3** and S-DABOC **4** within the NNIBP

that **3** assumed an orientation very similar to that of the co-crystallized inhibitor (MKC-442, emivirine) revealing the presence of specific interactions that could be responsible for the stability of the resulting inhibitor–RT complex: a hydrogen bond contact between the NH group at position 3 (in its tautomeric form) with the carbonyl moiety of Lys101 (region B in Figure 2) and profitable hydrophobic interactions between the alkyl side chain of Val106 and the C2 phenyl ring of the inhibitor which was accommodated into a large pocket mainly defined by Phe227, Pro225, Pro236, and Tyr318 (region C in Figure 2). Moreover, the side chains of both Lys103 and Val106 were also found at close contact with the pyrimidinone nucleus whereas the benzyl substituent at position C6 was embedded into an extended hydrophobic region defined by the aromatic side chains of Tyr181, Tyr188, Phe227, and Trp229 as well as by Leu100, Leu234, and Val179 (region A in Figure 2).

Additional molecular modeling studies revealed that the S-DABO cytosine analogue (S-DABOC) **4**, obtained from **3** after C4 chlorination and subsequent amination (Scheme 1), displayed almost the same interaction pattern of **3** within the al-

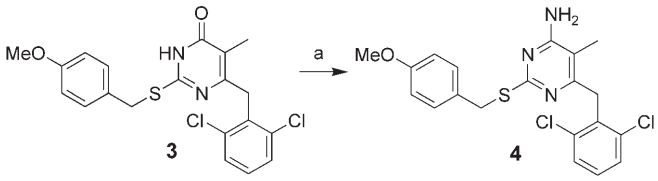

Scheme 1. Synthesis of the S-DABOC **4**: a) 1) $POCl_3$, 105 °C, 1 h; 2) $NH_{3(g)}$/MeOH, 90 °C, 2 h.

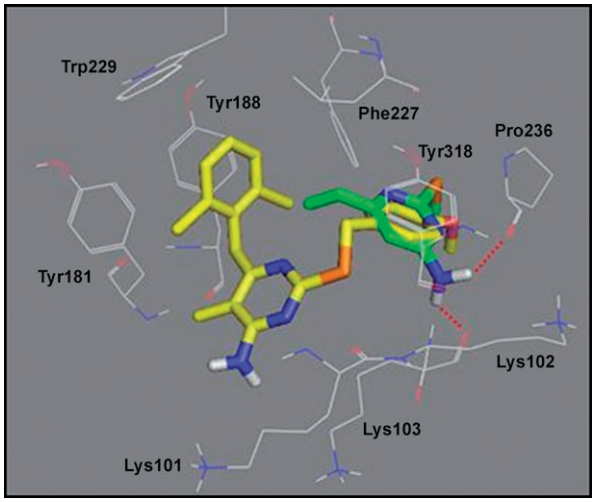

Figure 3. Superimposition of the energetically preferred docked conformations of **4** (yellow, sticks) and **10** within the NNIBP. Putative intermolecular hydrogen bond for **10** are highlighted by dashed lines.

losteric site of HIV-1 (wt) (see Figure 3). The lower potency of **4** against RT (wt) (see Table 1) was explained by the loss of a hydrogen bond contact between the NH group at position 3 of **3** and the carbonyl moiety of Lys 101. However, no dramatic loss of activity towards selected mutants was observed for the cytosine analogue.

Based on these observations, we decided to dismantle the structure of **4** and to start a systematic functionalization of the cytosine scaffold to identify the essential structural features required for RT inhibition. A valuable approach in overcoming drug resistance could consist of selecting the lower number of specific interactions within the allosteric site while maintaining a good affinity for the enzyme. A series of simplified analogues of **4** have been therefore generated and tested against HIV-1 (wt) and mutant strains.

Table 1. Anti-HIV-1 activity and cytotoxicity of compounds **3** and **4**.

	ID_{50}[a,b] [μM]			ED_{50} [μM][a,c]			
Compd	wt	K103N	Y181I	IRLL98[d]	K103N	Y181L	CC_{50}[e]
3	0.004	102	150	0.047	4.7	>32.3	32.3
4	0.046	150	180	4.95	39%	>59.5	>59.5

[a] Data represent mean values of at least two experiments. [b] ID_{50}: inhibiting dose 50 or dose needed to inhibit 50% of the enzyme. [c] ED_{50}: effective concentration 50 or concentration needed to inhibit 50% HIV-induced cell death, evaluated with the MTT method in MT-4 cells. [d] Clinical isolate resistant to NRTIs (lamivudine, emtricitabine) and NNRTIs (NVP, delavirdine, EFV). [e] CC_{50}: cytotoxic concentration 50 or concentration needed to induce 50% death of noninfected cells evaluated with the MTT method in MT-4 cells.

S-DABOCs

During the past 25 years, many different modifications have been performed on the pyrimidinone scaffold of the DABO-family with the aim of identifying new analogues able to target the NNRTIs drug resistant mutants: 1) introduction of different chains at position C2; 2) substitution of the hydrogen in C5 with bulkier groups; 3) introduction of different substituents on the phenyl ring at position C6; 4) substitution of the phenyl ring in C6 with different aromatic or heteroaromatic moieties.[5] To investigate the biological potentiality of the unexplored class of S-DABO cytosine analogues (S-DABOCs), we started with a major simplification of the lead **4** by removing the phenyl ring in C2, the methyl group in C5, and replacing the benzyl moiety in C6 with a vinyl group able to mantain π stacking interactions within the hydrophobic region A. Compound **5**, easily obtained following a previously optimized procedure,[18] was initially protected as tert-butyl dimethylsilyl derivative (**6**) and then reacted with thionyl chloride to give the expected compound **7** together with a small amount of the alcohol **8** (Scheme 2). Deprotection of compound **7** with TBAF gave the desired alcohol **8** which was then treated with methanolic ammonia affording the amino derivative **9**. The latter

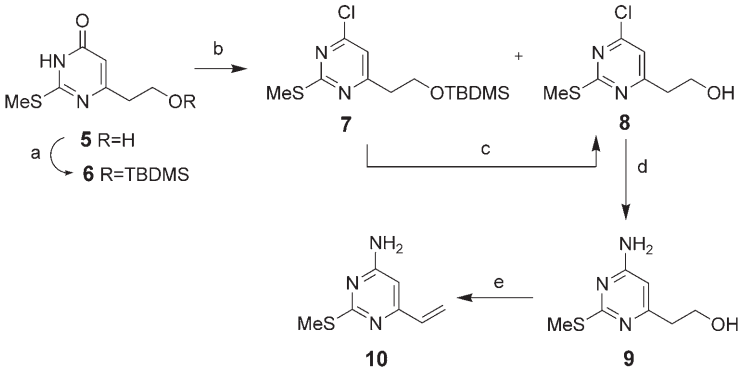

Scheme 2. Synthesis of the simplified analogue **10**: a) TBDMSCl, imidazole, DMF, RT, 1 h; b) $SOCl_2$, DMF, CH_2Cl_2, 40 min; c) TBAF, THF, RT, 1 h; d) TBAF, THF, RT, 1 h; e) $NH_{3(g)}$/MeOH, sealed tube, 90 °C, 3 h; f) NaH, dioxane, reflux, 3 h.

compound was finally dehydrated by refluxing in the presence of sodium hydride to give the simplified analogue **10**. However, from biological evaluation on isolated RT (wt), compound **10** resulted completely inactive (Table 2). At this point, we planned to functionalize the cytosine scaffold **10**, gradually reintroducing the structural key features required for the interaction of the lead compound **4** with the regions A and C previously described. To select the best substituents to be introduced into the cytosine scaffold, compound **10** was docked

Table 2. Anti HIV-1 activity and cytotoxicity of S-DABOC derivatives.

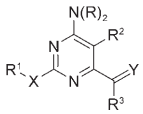

Compd	$N(R)_2$	R^1	R^2	R^3	X	Y	ID_{50}[a,b] [μM] wt	ED_{50} [μM][a,c] NL4-3 wt	K103N	Y181C	Y188L	CC_{50}[d]	Fold resistance[e] K103N	Y181C
10	NH_2	Me	H	H	S	CH_2	na[f]	> 29.94	> 29.94	> 29.94	> 29.94	> 29.94		
21a	NH_2	Me	H	4-F-Ph	S	O	42	nd[g]	nd	nd	nd	nd		
21b	NH_2	Et	H	4-F-Ph	S	O	na	nd	nd	nd	nd	nd		
21c	NH_2	Pr	H	4-F-Ph	S	O	na	nd	nd	nd	nd	nd		
22a	NH_2	Me	Me	4-F-Ph	S	O	2.1	0.58	5.96	0.21	> 90.25	> 90.25	10.3	0.36
22b	NH_2	Et	Me	4-F-Ph	S	O	na	7.35	> 17.18	48% at 17.18[h]	> 17.18	> 17.18		
22c	NH_2	Pr	Me	4-F-Ph	S	O	na	6.20	> 16.39	> 16.39	> 16.39	> 16.39		
25c	NMe_2	Me	Me	4-F-Ph	S	O	na	47% at 81.96	> 81.96	10.78	> 81.96	> 81.96		
27b	NH_2	Me	Me	4-F-Ph	S	CH_2	na	12.51	73.34	4.8	> 90.91	> 90.91		
27c	NMe_2	Me	Me	4-F-Ph	S	CH_2	na	> 8.25	> 8.25	> 8.25	> 8.25	8.25		
28	NMe_2	Me	Me	4-(Me_2N)-Ph	S	O	na	> 75.75	> 75.75	> 75.75	> 75.75	> 75.75		
30	NMe_2	Me	Me	4-(Me_2N)-Ph	S	CH_2	na	> 36.89	> 36.89	> 36.89	> 36.89	> 36.89		
NVP	–	–	–	–	–	–	0.4	0.08	1.8	0.87	5.6	> 100	22.5	10.9
EFV	–	–	–	–	–	–	0.04	0.004	0.09	0.006	0.23	> 0.3	22.5	1.5

[a] Data represent mean values of at least two experiments. [b] ID_{50}: inhibiting dose 50 or dose needed to inhibit 50% of the enzyme. [c] EC_{50}: effective concentration 50 or concentration needed to inhibit 50% HIV-induced cell death, evaluated with the MTT method in MT-4 cells. [d] CC_{50}: cytotoxic concentration 50 or concentration needed to induce 50% death of noninfected cells evaluated with the MTT method in MT-4 cells. [e] Fold resistance: ratio of EC_{50} value against drug-resistant strain and EC_{50} of the wild-type NL4-3 strain. [f] na: not active at 400 μM (the highest concentration tested). [g] nd: not determined. [h] Percent inhibition of HIV-induced cell death at the reported micromolar concentration.

into the NNIBP of RT (Figure 3).[19] Superimposition of the energetically preferred docked conformation for **4** and **10** revealed that the heterocyclic core of **10** was superposable with the C6 benzyl group of **4** allowing a π-π out of plane interaction with Tyr318. In addition, two hydrogen bond interactions between the amino group of **10** and the backbone carboxy group of Pro236 and Lys103 were found.

However, the loss of profitable interaction with the region B and C of the NNIBP may account for the complete loss of activity. The proposed binding mode for compound **10** allowed us to hypothesize that the introduction of a phenyl-carbonyl group in C6 instead of a benzyl group (such as in the lead **4**) may allow the formation of a profitable hydrogen bond contact with the hydroxy group of Tyr318.

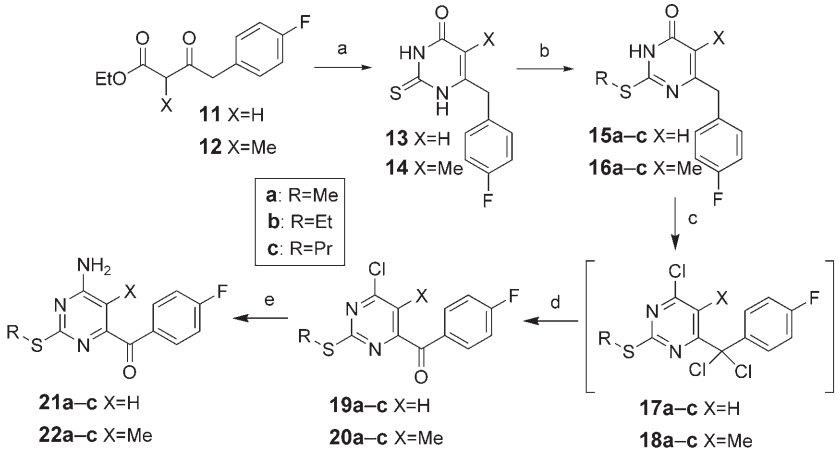

Scheme 3. Synthesis of simplified analogues **21a–c** and **22a–c**: a) thiourea, EtONa, reflux, overnight; b) RX, DMF, MW, 130 °C, 5 min; c) $SOCl_2$, DMF, $CHCl_3$, RT, 48 h; d) H_2O, 110 °C, 12 h; e) $NH_{3(g)}$/MeOH, 90 °C, 3 h.

Accordingly, the first synthetic approach used for the synthesis of such C6 aroyl analogues is depicted in Scheme 3. Condensation of the β-keto esters **11** and **12**[20] with thiourea in the presence of sodium ethoxide in refluxing ethanol, afforded the pyrimidinones **13** and **14** which were selectively *S*-alkylated by reaction with the appropriate alkyl halide under microwave irradiation to give the desired derivatives **15a–c** and **16a–c** (Scheme 3). Treatment of the latter compounds with thionyl chloride in DMF/chloroform led to the trichloroderivatives compounds **17a–c** and **18a–c** which were not isolated but simply refluxed in water to give **19a–c** and **20a–c** even if in low overall yields.

Finally, reacting compounds **19a–c** and **20a–c** with methanolic ammonia in a sealed tube gave the desired S-DABOC derivatives **21a–c** and **22a–c**. However, because of the low overall yields of the above described approach and taking into account that few modifications of the arylmethyl carbon at the C6 position of DABO analogues have been reported so far, our attention was focused on the search for an alternative and more versatile procedure. Accordingly, an efficient approach for the synthesis of C6 functionalized S-DABOCs has been re-

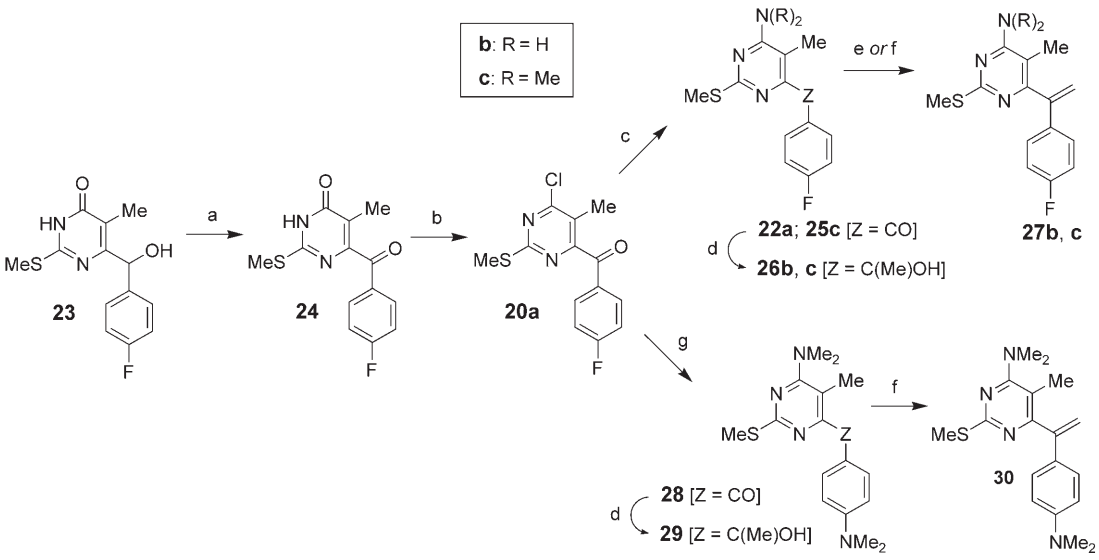

Scheme 4. Improved synthesis of C6 arylmethyl derivatives: a) Dess–Martin, CH_2Cl_2, 0 °C→RT, 2 h; b) $POCl_3$ reflux, 15 min; c) $NH_{3(g)}$/MeOH, 90 °C, 3 h (for **22a**) or $HNMe_2$, K_2CO_3, RT, 1 h (for **25c**); d) MeMgBr, THF, −15 °C→RT, 1 h; e) HCl conc., reflux, 30 min (for **27b**); f) 1) $(CF_3CO)_2O$, 2,6-lutidine, Et_2O, −5 °C→RT; 12 h; 2) AcOH, 60 °C, 30 min (for **27c**); g) $HNMe_2$, K_2CO_3, DMF, MW, 90 °C, 10 min.

cently developed.[21] The versatile intermediate **23**, obtained through a four step approach in 49% overall yield, can in fact be consecutively functionalized as shown in Scheme 4. Oxidation of **23** with Dess–Martin periodinane afforded the C6 aroyl derivatives **24** which was selectively chlorinated at C4 to give **20a**. Subsequent nucleophilic substitution on compound **20a** with the appropriate amine, gave the S-DABOC derivatives **22a** and **25c** in high yields. Further functionalization on the C6 arylmethyl carbon was introduced reacting these latter compounds with methylmagnesium bromide to give **26b** and **c** which were finally dehydrated to give the vinyl derivatives **27b** and **c**. It was also interesting to note that reaction of compound **20a** with dimethylamine under microwave irradiation, gave rise to the bis-substituted derivative **28** which was then transformed into the vinyl-derivative **30** by a Grignard reaction followed by dehydration.

The synthesized compounds were evaluated in enzymatic tests for their ability to inhibit RT (wt) and on MT-4 cells for cytotoxicity and anti-HIV activity (both on wild type and mutant strains) in comparison with nevirapine (NEV) and efavirenz (EFV), used as reference drugs (Table 2). In particular the following mutants were used for cellular testing: K103N, Y181C, and Y188L. As expected, results showed that the contemporary introduction of a phenyl-carbonyl group in C6 and of a methyl group in C5 resulted into an interesting lead compound (**22a**) possessing low cytotoxicity and submicromolar activity on MT-4 cells infected with both HIV-1 (wt) and clinically relevant mutants. It was also interesting to note that removal of the C5 methyl group (compound **21a**) determined a reduction of the antiviral potency whereas increasing the length of the alkylic chain in C2 (compounds **20b** and **c** and **21b** and **c**) led to a complete loss of activity independently from the presence of the methyl group in C5. In addition, the relevance of the C4 amino group was highlighted by the loss of activity consequent to its replacement with a dimethylamino moiety (compounds **25c**, **27c**, **28**, and **30**) and by the complete inactivity of the S-DABO intermediate **23**.[22]

As shown in Table 2, biological data showed some contradictions between ID_{50} and ED_{50} values for several compounds, probably due to the fact that cellular tests reflect the interference of a compound in viral steps not shown in the pure RT enzymatic tests. In particular, compound **27b** bearing a vinyl group in C6 in place of the carbonyl moiety, was inactive in enzymatic tests whereas moderate activity was detected in cells infected with both wild type and Y181C mutant strain.

To rationalize the SAR for this new class of S-DABOC derivatives, the synthesized compounds were docked into the NNIBP of RT (wt) (see Figure 4). The interesting activity profile of **22a**

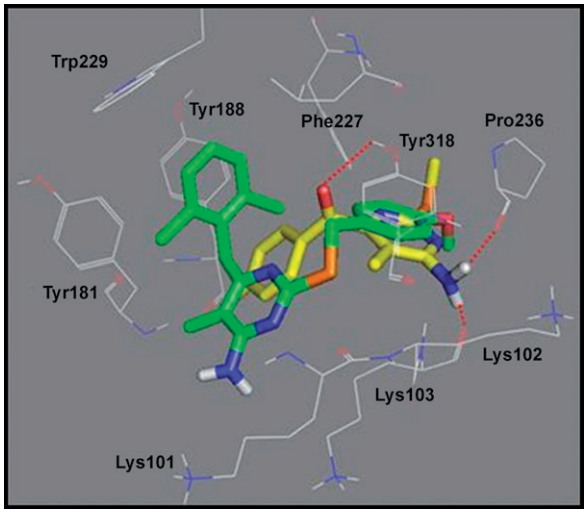

Figure 4. Superimposition of the energetically preferred docked conformations of **22a** (yellow, sticks) and **4** (green, sticks) within the NNIBP. Putative intermolecular hydrogen bond for **22a** are highlighted by dashed lines.

can be then justified on the basis of the predicted favorable interactions within the NNIBP: two hydrogen bond contact between the C4 amino group and the backbone carboxy group of Pro 236 and Lys 103; an additional hydrogen bond interaction between the C6 carboxy group and Tyr 318, π-π out of plane interaction with Tyr 318. In addition, the C5 methyl group was accommodated into an hydrophobic region defined by Leu 100, K 102, and Tyr 318. On the basis of the predicted bind mode for all the other S-DABOC derivatives, the biological results can be fully justified with the loss of specific interactions within the NNIBP.

In summary, this results fully support the experimental activity of **22a** and confirm our speculations about the possibility of selecting the lowest number of specific interactions within the NNIBP for the synthesis of novel NNRTIs able to overcome drug resistant mutations. In terms of relative resistance (that is, fold reduced activity, see Table 2), **22a** was superior to both nevirapine and efavirenz, however in terms of absolute potencies it was similar to NVP and less potent than EFV. Exploitation of the above described synthetic procedure is underway in our laboratories to synthesize a large number of S-DABOC analogues hopefully endowed with an increased affinity for RT.

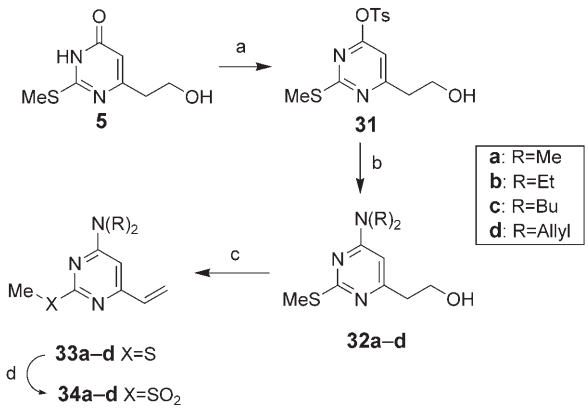

Scheme 5. Synthesis of simplified analogues **33a–d** and **34a–d**: a) TsCl, DMAP, CH_2Cl_2, RT, 10 min; b) 1) R_2NH, THF, reflux, 360 rpm, overnight; 2) PS-1,3,4,6,7,8-hexahydro-2*H*-pyrimido[1,2-a]pyrimidine; 3) PS-isocyanate; c) NaH, dioxane, reflux, 360 rpm, 3 h; d) oxone, MeOH/H_2O, 360 rpm, RT, 3 h.

DAVPs

In parallel with the research on S-DABOC derivatives, the synthesis of additional simplified analogues of compound **4** had been focused on the functionalization of the C4 position of the pharmacophoric structure **10**. The combinatorial approach used for the introduction of different amines on the C4 of the pyrimidine core is shown in Scheme 5:[23] only a selection of the most representative compounds is herein reported (see Table 3).

Compound **31**, obtained reacting the alcohol **5** with tosyl chloride, was submitted to a three-step parallel solution phase procedure. In the first step, **31** was partitioned into separate reaction vessels and reacted with different amines; once all the reactions were at completion, two solid-supported scavengers were added to remove excess reagents and side products. The PS-1,3,4,6,7,8-hexahydro-2*H*-pyrimido[1,2-a]pyrimidine scavenger was added to remove the *p*-toluenesulfonic acid released in the reaction medium as side product, while the excess of secondary amines was removed using a PS-isocyanate scavenger. After simple parallel filtration, compounds **32a–d** were obtained in more than 95% purity (as shown by HPLC/MS analysis) and then dehydrated by reaction with NaH in refluxing dioxane.

After removing volatiles under reduced pressure, the reaction mixtures were taken up in CH_2Cl_2 and subjected to parallel filtration to afford compounds **33a–d** as pure products. Finally, compounds **33a–d** were selectively converted into corresponding sulfones **34a–d**, by treatment with oxone, which was previously reported to be very efficient for selective sulfur oxidation.[24] The electron withdrawing sulfone group seems to

Table 3. Anti-HIV-1 activity of DAVP derivatives.

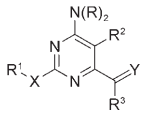

Compd	$N(R)_2$	R^1	R^2	R^3	X	Y	ID_{50} [μM][a,b] wt	K103N	Y181I
33a	$N(Me)_2$	Me	H	H	S	CH_2	na[c]	na	na
33b	$N(Et)_2$	Me	H	H	S	CH_2	na	na	na
33c	$N(Bu)_2$	Me	H	H	S	CH_2	na	na	na
33d	$N(Allyl)_2$	Me	H	H	S	CH_2	na	na	na
34a	$N(Me)_2$	Me	H	H	SO_2	CH_2	0.022	28	78
34b	$N(Et)_2$	Me	H	H	SO_2	CH_2	21.3	na	na
34c	$N(Bu)_2$	Me	H	H	SO_2	CH_2	160	na	na
34d	$N(Allyl)_2$	Me	H	H	SO_2	CH_2	na	na	na
37	$N(Me)_2$	MeNH	H	H	–	CH_2	na	na	na
39	$N(Me)_2$	$MeSO_2NH$	H	H	–	CH_2	na	na	na
42a	$N(Me)_2$	4-MeO-Bn	H	H	S	CH_2	3.1	na	na
42b	$N(Me)_2$	4-CN-Bn	H	H	S	CH_2	na	na	na
43a	$N(Me)_2$	4-MeO-Bn	H	H	SO_2	CH_2	na	na	na
43b	$N(Me)_2$	4-CN-Bn	H	H	SO_2	CH_2	na	na	na
47a	$N(Me)_2$	Me	Cl	H	S	CH_2	130	na	na
47b	$N(Me)_2$	Me	Br	H	S	CH_2	5.09	na	na
47c	$N(Me)_2$	Me	I	H	S	CH_2	na	na	na
48a	$N(Me)_2$	Me	Cl	H	SO_2	CH_2	na	na	na
48b	$N(Me)_2$	Me	Br	H	SO_2	CH_2	1.56	na	na
48c	$N(Me)_2$	Me	I	H	SO_2	CH_2	275	na	na

[a] Data represent mean values of at least two experiments. [b] ID_{50}: inhibiting dose 50 or dose needed to inhibit 50% of the enzyme. [c] na: not active at 400 μM (the highest concentration tested)

play an important role in activating the C6 vinyl moiety towards Michael addition reactions and could therefore determine peculiar interactions within the NNIBP. A preliminary biological screening of this combinatorial library against isolated RT (see Table 3) revealed that, whereas the sulfides **33a–d** were completely inactive, the sulfones **34a–c** displayed an interesting antiviral activity. Moreover, a direct correlation was found between the size of the C4 substituent and the ID_{50} values for the sulfone derivatives: the antiviral activity is inversely related to the bulkiness of the C4 substituent, with the 4-dimethylamino-6-vinylpyrimidine derivative (DAVP) **34a** as the most active inhibitor. To draw a complete SAR map for this new class of derivatives, a systematic functionalization of the DAVP scaffold was started: keeping fixed the dimethylamino group at C4 position and the C6 vinyl moiety, the introduction of different substituent on the C2 position of the pyrimidine nucleus by nucleophilic displacement of the C2 methyl sulfone was first explored. However, because of the sulfone mediated activation of the C6 vinyl group, direct C2 functionalization of compound **34a** resulted in a nucleophilic addition to the double bond.

To obtain the expected C2 functionalized derivatives, we started from the alcohol **32a** which was first oxidized to the corresponding sulfone **35** and then submitted to nucleophilic substitution: reacting **35** with methylamine under microwave irradiation gave the 2-methylamino derivative **36** which was converted into the final compound **37** upon dehydration with sodium hydride (Scheme 6). Nucleophilic substitution on **35**

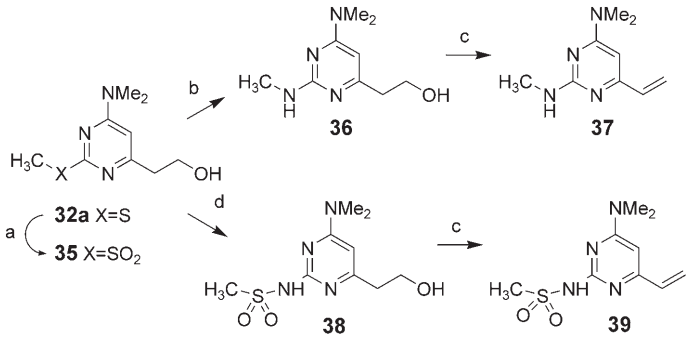

Scheme 6. Synthesis of simplified analogues **38** and **39**: a) *m*CPBA, CH_2Cl_2, RT, 4 h; b) CH_3NH_2, MW, 130 °C, 30 min; c) NaH, dioxane, reflux, 5 h; d) $CH_3SO_2NH_2$, NaH, DMF, MW, 120 °C, 20 min.

with methanesulfonamide and subsequent dehydration with sodium hydride gave instead the desired 2-methylsulfonamido derivative **39**. Moreover, to introduce in C2 a benzyl substituent such as in compound **4**, the sulfone **35** was reacted with aqueous solution of sodium hydrosulfide to give the thiol derivative **40** (Scheme 7). Selective *S*-benzylation of the latter compound under microwave irradiation with the appropriate benzyl halide afforded the C2 substituted compounds **41a** and **b** which were first transformed into the corresponding 6-vinyl derivatives **42a** and **b** and finally oxidized to give the sulfones

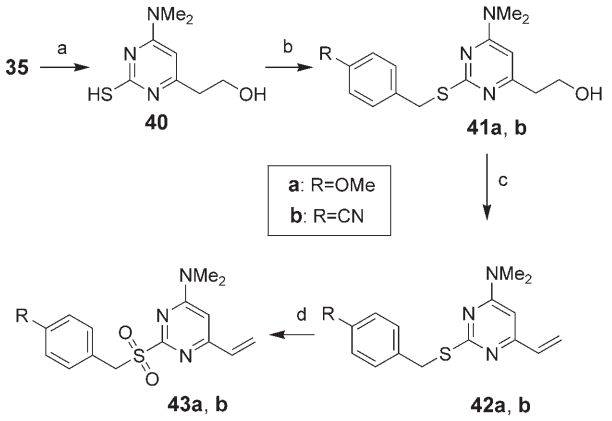

Scheme 7. Synthesis of simplified analogues **42a** and **b** and **43a** and **b**: a) NaSH, H_2O, reflux, 2 h; b) 4-MeO-benzylchloride (for **41a**) or 4-CN-benzylbromide (for **41b**), K_2CO_3, DMF, MW, 130 °C, 5 min.; c) NaH, dioxane, reflux, 3 h; d) oxone, MeOH/H_2O, RT, overnight.

43a and **b**. Subsequently, the functionalization of position C5 was investigated: compound **5** was transformed into the corresponding 5-halo derivatives **44a–c** using the appropriate halogenating agent under microwave assisted conditions (Scheme 8).[25]

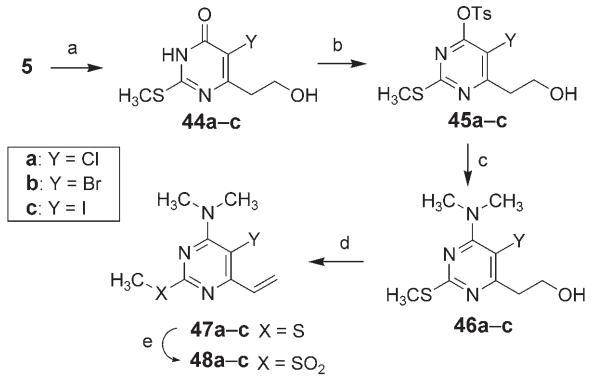

Scheme 8. Synthesis of simplified analogues **47a–c** and **48a–c**: a) NCS (for **44a**), NBS (for **44b**), or ICl (for **44c**), DMF, MW, 50 °C, 15 min; b) TsCl, DMAP, CH_2Cl_2, RT; c) Me_2NH, EtOH, K_2CO_3, reflux, 1 h; d) NaH, dioxane, reflux, 3 h; e) oxone, MeOH/H_2O, RT, overnight.

Submitting the latter compounds to the same synthetic sequence depicted in Scheme 5, the desired C5 substituted derivatives **47a–c** and **48a–c** were obtained. Biological evaluation of the DAVP analogues against isolated RT (wild type and mutants) revealed that severe structural requirements are needed for RT inhibition (see Table 3). The most active compound (**34a**) is characterized by the simultaneous presence of a small dimethylamino group in C4, a C2 methylsulfonyl moiety, and a C6 vinyl group. Increasing the bulkiness in C4 (compounds **34b–d**) determined a reduction of ID_{50} whereas replacing the C2 sulfone with a sulfide (**33a–d**) determined a complete loss of activity. The functionalization in C2, generally lead to inactive compounds with the only exception of **42a** which showed a moderate activity whereas the functionaliza-

tion in C5 (compounds **47a–c** and **48a–c**) determined a loss of potency. Despite the discouraging biological results obtained from the functionalization of the lead compound **34a**, the need for further exploration can be justified on the basis of the unprecedented behavior shown by these compounds (see next paragraphs).

Contrary to the NNRTIs reported to date, DAVP derivatives were in fact found to inhibit HIV-1 reverse transcriptase (RT) by a competitive mechanism with the nucleotide substrate after binding to the non-nucleoside inhibitors binding pocket (NNIBP) of the free enzyme.[27]

DAVPs are competitive inhibitors of HIV-1 RT with respect to the nucleotide substrate

All of the known NNRTIs are allosteric inhibitors which display a fully or mixed non-competitive type of inhibition (with respect to both the DNA-template and dNTPs) of the polymerization reaction catalyzed by HIV-1 RT.[28] Presteady state kinetic analysis of the reaction catalyzed by HIV-1 RT in the absence or in the presence of NNRTIs showed that the inhibition is due to a great reduction of the polymerization rate k_{pol}[29] To determine the mechanism of inhibition of selected DAVP derivatives, they were titrated in in vitro reverse transcription assays in the presence of varying concentrations of either the nucleic acid or the nucleotide substrates. As a result, inhibition exerted by the tested compounds was sensitive to changes in the nucleotide concentration (Figure 5, panels B, E, F, G), resulting in an increase of the apparent K_m for dTTP (Figure 5, panel C, H, I, J). On the other hand, no effect on RT inhibition was observed when the nucleic acid concentration was varied.[30] These results clearly indicate that the tested DAVPs are competitive inhibitors of RT with respect to the nucleotide substrate. As a comparison, the structurally related 1-[(2-hydroxyethoxy)methyl]-6-(phenylthio)thymine (HEPT) analogue TNK-651 showed a purely noncompetitive mechanism of inhibition with respect to the nucleotide substrate, as shown by the lack of significant variations in the apparent K_m value for dTTP, both with the RT wild-type and the K103N mutant (Figure 5, panel D).

DAVPs bind to the NNIBP

All of the known NNRTIs bind to a specific site or pocket (NNIBP) in the RT heterodimer, close to but distinct from the catalytic site. However, given the peculiar mechanism of action shown by the DAVPs, it is possible that such compounds bind to a different site. In the absence of co-crystals between RT and our compounds, we have obtained indirect evidences of their binding site by testing their sensitivity to known NNRTIs-resistant mutations, localized in the NNIBP.[31–33] The affinity of the lead compound **34a** for the enzyme was in fact strongly affected by mutations K103N and Y181I (Figure 5, panel A). However, it is important to note that compound **34a** still retained measurable activity against both mutants, even though lower than against the wild-type enzyme. Moreover, when **34a** was also tested against the mutants L100I and V179D, no significant loss of activity was observed (Figure 5, panel A). These results support the conclusion that the DAVP **34a** binds to the NNIBP and act therefore as nonclassical competitive inhibitor: characteristics of this mode of inhibition are both a reduced affinity of the enzyme for the substrate (increase of K_m in Figure 5, panel C) and the reduction of the inhibitors' effect consequent to the increase of the substrate concentration (and vice versa; Figure 5, panel A).

Kinetics of the binding of 34a to wild-type and mutant HIV-1 RT.

To get further insight into the mechanism of interaction between DAVPs and HIV-1 RT, the kinetics of the binding of **34a** to different RT–substrate complexes were determined. HIV-1 RT exists in three forms along its reaction pathway: the free enzyme, the binary complex with the nucleic acid as the substrate, and the catalytically competent ternary complex with both the substrates represented by the nucleic acid and the 2′-deoxynucleotide. As revealed by their crystal structures, these three forms are not equivalent, as HIV-1 RT undergoes sequential structural rearrangements upon binding it's substrates.[28] As summarized in Table 4, compound **34a** showed a 13-fold faster association (k_{on}) and eightfold faster dissociation (k_{off}) rates in the case of the binary RT–DNA complex with respect to the free enzyme. Thus, even though the equilibrium dissociation constant ($K_i = k_{off}/k_{on}$) for these two enzymatic forms is the same, the analysis of the binding constants suggests that binding of the nucleic acid stabilizes the binding site in a more open conformation, which allows for a faster association of the inhibitor to the enzyme, but also for a faster dissociation. When the same analysis was applied to the ternary complex of RT with both the nucleic acid and the 2′-deoxynucleotide, a tenfold decrease in the association rate with respect to the free enzyme and a 140-fold decrease in the association rate with respect to the binary complex were observed. On the other hand, the dissociation rate from the ternary complex was not significantly different from those calculated for the other enzymatic forms. In summary, these results indicate that the formation of the ternary complex upon binding of the 2′-deoxynucleotide causes a "closure" of the binding site that is now accessible only at a very slow rate. Moreover the kinetic analysis clearly shows that the binding of **34a** to the free enzyme is more stable compared to the binding with the other forms, thus allowing exclusion of a classical competitive inhibition which might result only in the case that the inhibitor binds exclusively to the catalytic site of the binary complex (as the nucleotide does). To the best of our knowledge, DAVPs are the first NNRTIs reported to date to exhibit such a behavior.

DAVPs are not irreversible inhibitors of RT

As previously reported,[23] the introduction of a sulfone moiety in the C2 position of 6-vinylpyrimidine derivatives is able to confer Michael acceptor properties, suggesting a possible irreversible conjugate addition to nucleophilic functional group of a side chain of the enzyme. However, several considerations

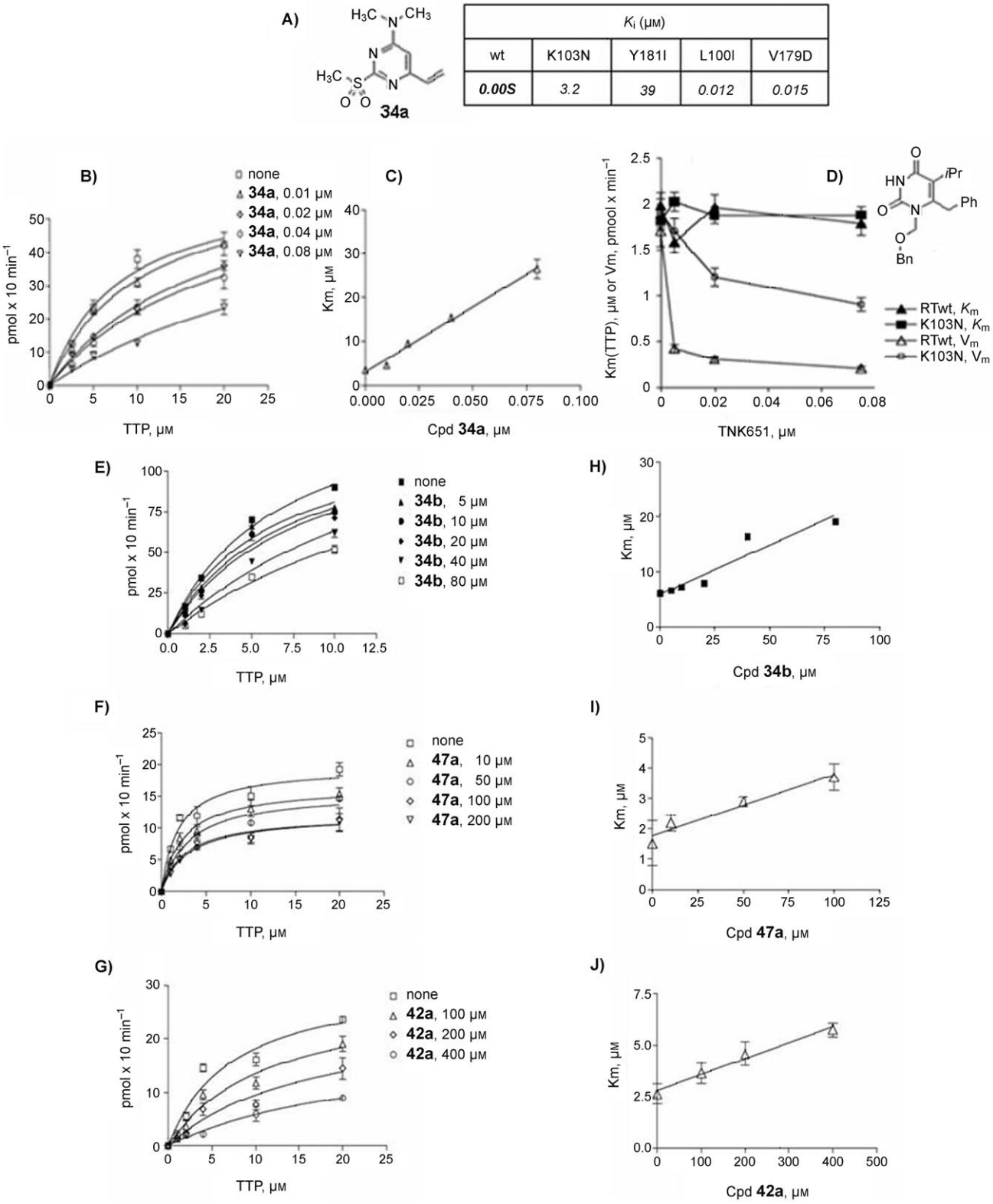

Figure 5. A) Affinity of compound **34a** for RT wild type and drug-resistant mutants. B) Plot of the incorporation rates of wild-type HIV-1 RT reporting the variation of the reaction rate as a function of the dTTP substrate concentration in the absence or in the presence of increasing amounts of compound **34a**. Curves were fitted to a Briggs-Haldane mechanism. Error bars represent ±SD of three independent replicates. C) Variation of the apparent affinity (K_m) for the nucleotide substrate as a function of the concentration of **34a**. K_m values were determined as described in the experimental section from the curves shown in panel B; D) Variations of the apparent affinity (K_m, filled symbols) and maximal velocity (V_m, open symbols) for dTTP incorporation catalyzed by HIV-1 RT wild type (triangles) or K103N (squares) as a function of TNK-651 concentration.[26] Data are the means of three independent replicates. Bars represent ±SD; (E, F, G) Experiments were performed as in panel B, but in the absence or in the presence of increasing amounts of compound **34b**, **47a**, and **42a**, respectively; (H, I, J) Experiments were performed as in panel C, but in the absence or in the presence of increasing amounts of compound **34b**, **47a**, and **42a**, respectively.

Table 4. Kinetics of the binding of **34a** to RT (wt).

Enzymatic form								
RT			RT–DNA			RT–DNA–dNTP		
K_i [nM]	k_{on}[a] [$M^{-1}s^{-1}$]	k_{off}[b] [s^{-1}]	K_i [nM]	k_{on}[a] [$M^{-1}s^{-1}$]	k_{off}[b] [s^{-1}]	K_i [nM]	k_{on}[a] [$M^{-1}s^{-1}$]	k_{off}[b] [s^{-1}]
8 (±1)	1.04×10^4 (±0.01)	8.4×10^{-5} (±0.4)	8 (±1)	14×10^4 (±1)	1.1×10^{-3} (±0.002)	16 (±1)	0.1×10^4 (±0.02)	1.6×10^{-5} (±0.1)

[a] Calculated from $k_{app}=k_{on}(K_i+[I])$ [b] Calculated from $k_{off}=K_i k_{on}$ [c] Due to the competitive nature of inhibition by **34a**, $K_{iapp}=K_i(1+([dNTP]/K_{mdNTP}))$, where [dNTP] is the nucleotide concentration used in the binding assay, and K_{mdNTP} is the apparent affinity of HIV-1 RT for the nucleotide. In this case, [dNTP] was kept equal to K_{mdNTP}, so that $K_{iapp}=2K_i$.

allow to exclude that our compounds are irreversible inhibitors of HIV-1 RT.

First, as an irreversible inhibitor acts through the permanent inactivation of the enzyme, it causes a decrease in the amount of enzyme available for the reaction. This will appear, under steady-state conditions, as non-competitive inhibition. However, the studied compounds are competitive toward one of the substrates, arguing that the inhibition is not irreversible.

Second, very often, irreversible inhibition is time-dependent and it is possible to measure the rate of enzyme inactivation as a function of time. In detail, because no dissociation of an irreversible inhibitor is possible from the enzyme, a time-dependent accumulation of irreversibly inactivated enzyme, occurs. However, no time-dependent effects were observed for our inhibitors when they were preincubated for increasing times in the presence of the enzyme,[34] suggesting a rapid equilibrium between free RT and the RT–inhibitor complex.

A final consideration is that, for an inhibitor with an affinity as high as that of compound **34a**, irreversible inhibition should reduce stoichiometrically the concentration of the active enzyme. As a consequence, a linear relationship between enzyme concentration and affinity of inhibitors should be observed (that is, inhibitors with higher affinity cause higher reduction of the concentration of the active enzyme). We have checked for this occurrence and found no obvious effect of our compounds on the concentration of the active enzyme.

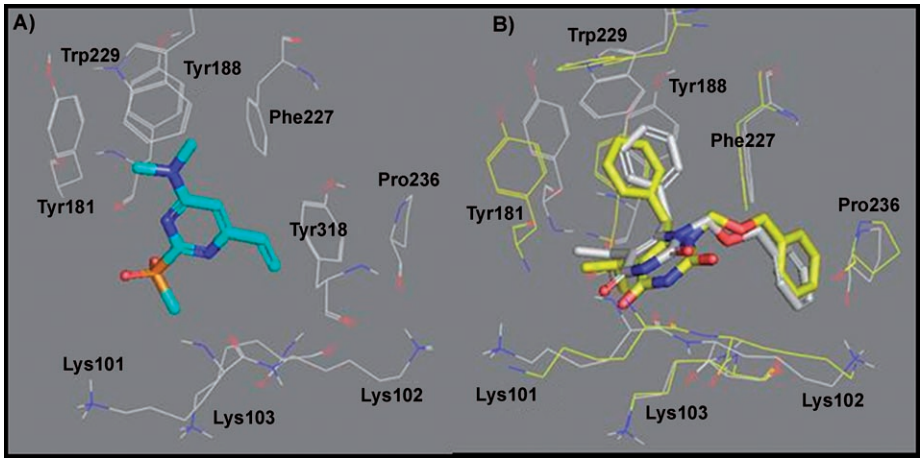

Figure 6. A) Docking of **34a** (thick lines) into the NNIBP of TNK-651–HIV-1 RT complex. B) Comparison of the docked TNK-651 (white carbons, thick lines) and X-ray conformation of TNK-651 (yellow carbons, thick lines) into NNIBP.

Docking studies of 34a with wild-type HIV-1 RT.

Compound **34a**, was docked into the wild-type HIV-1 RT NNIBP (Figure 6A). The coordinates of RT were obtained from the X-ray structure of the TNK-651–HIV-1 RT complex (PDB code 1RT2),[7] based on the similarity between DAVPs and TNK-651. Complexes generated by docking simulations were then refined with MacroModel. The reliability of the docking protocol was tested on the prediction of the binding geometries of the reference compound TNK-651 into the NNIBP. As a result, the experimental binding conformation of the reference drug was successfully reproduced with acceptable root-mean-square deviation (0.966 Å) of atom coordinates (see Figure 6B). Similarly, efavirenz was docked into the unliganded X-ray structure of efavirenz–HIV-1 RT (PDB code 1IKW).[35] The best docking orientation was practically coincident with that found in the crystal structure. The energetically preferred docked conformation of **34a** reveals interactions that may contribute to the stability of the resulting inhibitor–RT complex. The heterocyclic ring of the ligand is found at close contact with Tyr188, Tyr181, and Phe227 (allowing π-π interactions), whereas the vinyl group interacts with Tyr318. Moreover, additional profitable hydrophobic contacts between the methyl groups of the amine moiety and Trp229, are noted. The very polar sulfone group is oriented toward the water-exposed surface, in proximity of the positive charge of the Lys101 ammonium group.

Molecular dynamics simulations.

To check the reliability of the proposed binding mode of compound **34a**, MD simulations were carried out for the **34a**–wild-type RT complex. As our docking studies suggest that residues

Tyr188, Tyr181, and Tyr318 play an important role in the inhibition process, the distances between these amino acids and the ligand have been monitored. As the simulation progresses, a shortening of these distances can be appreciated, thus showing the binding pocket to close on the inhibitor **34a** (Figure 7).

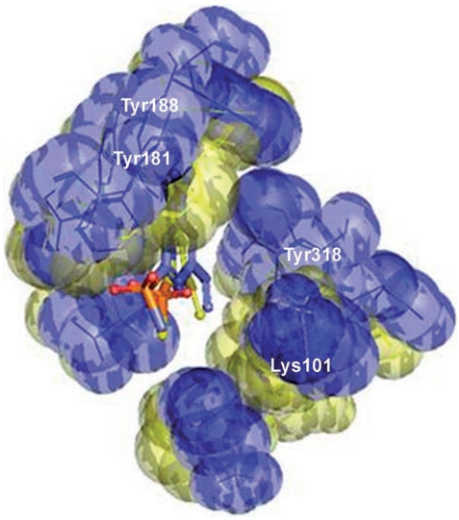

Figure 7. Overlap of **34a**–RT complexes prior (carbon atoms in blue) and after (carbon atoms and spheres in yellow) the MD simulations. For reason of clarity, only the side chains of the RT active site are represented as thin lines.

Moreover, an interesting movement of Lys101 toward the sulfone group of the inhibitor was identified, suggesting the possible formation of a hydrogen bond network also involving water molecules at the entry channel of the NNIBP.[36]

Structural and molecular basis for the inhibitory mechanism of DAVPs

The proposed pathway for the polymerization process catalyzed by reverse transcriptase involves the sequential binding of RT with DNA, and then with dNTP, followed by a nucleophilic attack that leads to the formation of a phosphodiester bond, with subsequent release of the pyrophosphate moiety.[37] The most important interactions that occur in the early phase of this process involve residues of the palm, thumb, and fingers of the p66 subunit: these structural elements act as a clamp, to position the nucleic acid chain relative to the polymerase active site. One of the residues playing a key role in the positioning of the template is Met230 which, interacting with the 3′ nucleotides of the primer strand, contributes to maintain the primer terminus in an orientation appropriate for a nucleophilic attack on the incoming deoxynucleoside triphosphate. The incorporation of the incoming nucleotide 5′-triphosphate into the growing viral DNA is catalyzed by the aspartic acid triad (Asp110, Asp185, and Asp186): while Asp110 and Asp186 interact with the β- and γ-phosphates of the dNTP by bivalent coordination of a Mg^{2+} ion, Asp185 activates the α-phosphate for the nucleophilic attack to the 3′-OH group of the primer by chelation of a second Mg^{2+} ion. To shed light on the peculiar mechanism of action exerted by DAVPs, the progression of the conformational changes in the side chain of Met230, Asp110, Asp185, and Asp186 during the MD simulations were monitored. In the case of **34a**–RT complex, it was clearly seen that, as the simulation progresses, the side chain of Met230 achieves an extended conformation (Figure 8A, white to blue). This new conformation could affect the positioning of the growing viral DNA (forcing the growing nucleic acid chain to reorient) and the subsequent polymerization process. By monitoring the conformational changes of the aspartic acid triad during the same simulations, it was interesting to note that, as the simulation progresses, the catalytic site opens so that the Asp185 side chain is gradually shifted 5.59 Å away from its initial position (Figure 8A, white to blue). Having these results in our hands, we carried out MD simulations on the **34b**–wild-type RT complex. The catalytic site triad also opened during the simulations. Nevertheless, this distortion was smaller than that observed for the most active compound (**34a**), as the Asp185 side chain extended only 3.52 Å away from its initial position and could once more give account for its reduced activity (Figure 8B). From a detailed analysis of the MD simulations it was therefore highlighted that DAVPs **34a** and **34b** determine similar conformational rearrangements on Met230 and Asp185 that play a key role in the polymerization process catalyzed from the RT. It is also noteworthy that the precise geometry of the aspartic acid side chains is critical for enzymatic activity as a single methylene extension of the carboxylic group (Asp to Glu) at any site in the aspartic triad produced inactive enzymes.[38] Structural comparisons of unliganded RT and complexed with NNRTIs have revealed that NNRTI binding induces long- and short-range structural distortions, including the conformational changes of the primer grip, which restricts the flex-

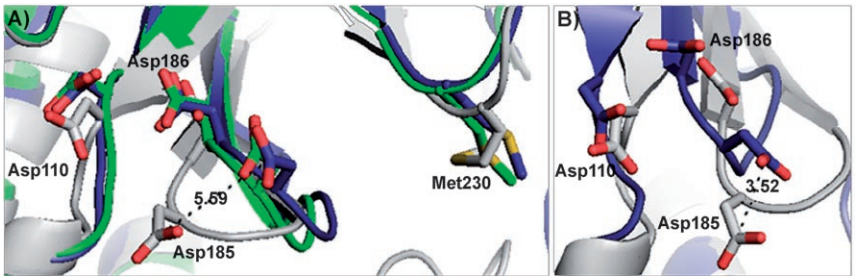

Figure 8. Overlay of representative snapshots from the MD trajectory showing the evolution of the position of relevant RT amino acid residues: A) **34a**–RT complex, side chains of Met230, Asp110, Asp185, and Asp186 are shown as sticks. Ribbons and carbon atoms of the side chains of these amino acids are colored according to time frames in the order white→green→blue (0, 500, and 1000 ps, respectively); B) **34b**–RT complex, ribbons and side-chain carbon atoms are colored according to time frames in the order white→blue (0 and 1000 ps, respectively).

ibility and mobility of the thumb domain and locks it in an open position.[10,41,42] Whatever the mechanism of inhibition, it is likely to be similar for the various non-nucleoside inhibitors and it is important to note that binding of non-nucleoside inhibitors to HIV-1 RT does not markedly decrease binding of template-primer or dNTP substrates.[43] It is therefore reasonable to expect that comparing the structures of unliganded HIV-1 RT with those of HIV-1 RT complexed with common NNRTIs and with the output of our MD simulations, should yield valuable insights into the peculiar mechanisms of action of DAVPs described herein. Superposition analysis depicted in Figure 9 clearly shows that the binding of common first- and second-generation NNRTIs (TNK-651, efavirenz, nevirapine, and R185545) to the RT-NNIBP determines only a major shift of the primer grip (Asp 230) whereas the aspartic acid triad does not seem to experience substantial modification compared to the unliganded enzyme. By contrast, it was interesting to note that the binding of compound **34a** to the NNIBP (**34a**–RT complex at t = 1000 ps) determines a different pattern of conformational changes: the side chain of Met 230 seems to adopt an extended conformation, whereas Asp 185 undergoes a significant and peculiar shift away from the aspartic acid triad (white circles in Figure 9) (that is, 7.66 Å away from its position in the TNK-651–RT complex). On the basis of these observations, it is reasonable to argue that the unusual shift of Asp 185 could be ultimately responsible for the competitive mechanism of action exerted by DAVP derivatives, as the magnesium ions in the catalytic site may lie so far apart, when **34a** is bound to the allosteric site, that no phosphodiester bond formation can take place. From a visual inspection of the polymerase active site, we can moreover speculate that the conformational rearrangements responsible for the competitive mechanism of action may originate from the disruption of the typical type II geometry of the β-turn formed by the conserved Tyr-Met-Asp-Asp sequence (residues 183–186), responsible for the correct positioning of the aspartate residues of the catalytic site (Figure 10).

In fact, it is well known that the formation of a hydrogen bond between Gln 182 and Met 184 is required for the stabilization of this otherwise strained type II conformation of this turn in the wild-type RT (Figure 9a). In a similar way, the complex RT–TNK-651 retained the Gln 182–Met 184 hydrogen bond and, consequently, displayed the same strained type II geometry of the β-turn (Figure 9c). On the contrary, in the **34a**–RT complex, a conformational rearrangement of the β-turn occurred so that the side chains of Asp 185 and Glu 182 were shifted far away from their original position (Figure 10b). As a consequence, the unfavorable steric interaction between the Cβ atom of Met 184 and the amide group of Asp 185 disappeared and the hydrogen bond between Gln 182 and Met 184

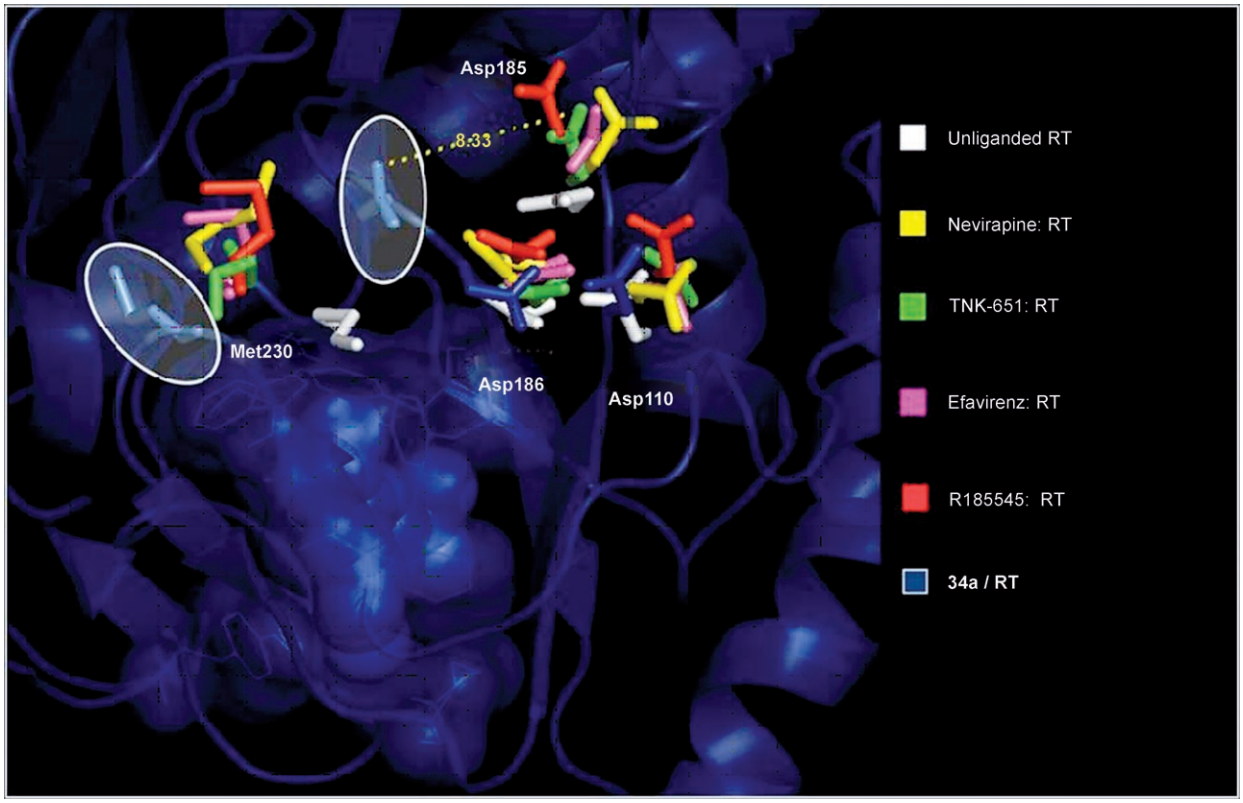

Figure 9. Superimposition of the structures corresponding to the **34a**–RT complex (blue) at t = 1000 ps, TNK-651–RT complex (green, PDB code 1RT2),[7] efavirenz–RT complex (violet, PDB code 1IKW),[34] nevirapine–RT complex (yellow, PDB code 3HVT),[39] R185545–RT complex (red, PDB code 1SUQ),[40] unliganded RT (white, PDB code 1HMV).[41] White circles highlight the conformational rearrangements of Met 230 and Asp 185 for the **34a**–RT complex in comparison to the other inhibitor–RT complexes. For reasons of clarity only the fundamental residues (Met 230, Asp 110, Asp 185, and Asp 186) of unliganded RT and RT complexed with reference inhibitors are shown as sticks. Compound **34a** bound to the NNIBP is shown as blue spheres.

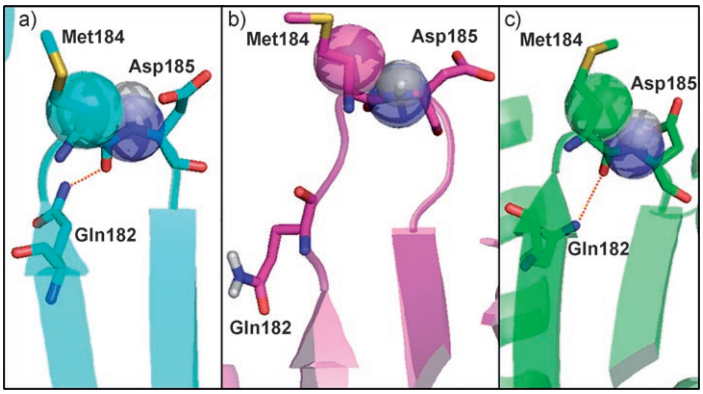

Figure 10. Structure of the β-turn (ribbons) around the active site of RT. Steric interactions between *C*-β atom of Met 184 and the amide group of Asp 185 (represented by means of transparent spheres) and hydrogen bonds (dotted red lines) can be appreciated. a) unliganded RT (cyan, PDB code 1HMV); b) **34a**–RT complex (magenta, at t = 1000 ps); c) TNK-651-RT complex (green, PDB code 1RT2). All figures were produced with Pymol.[44]

was lost. This result further supports the peculiar behavior of compound **34a**, which is able to induce conformational modifications not found in complexes between RT and common NNRTIs.

Conclusion

In summary, the present work describes a multidisciplinary approach for the identification of two novel classes of NNRTIs belonging to the S-DABO family: S-DABO cytosine analogues (S-DABOCs) and 4-dimethyamino-6-vinylpyrimidines (DAVPs). On the basis of the biological results obtained from the screening of our internal collection of S-DABO derivatives, a series of simplified analogues have been synthesized by systematic functionalization of the pyrimidine scaffold to identify the minimal required structural features for RT inhibition.

Starting from the highly simplified cytosine derivative **10**, molecular modeling was used to evaluate the structural determinants for RT–inhibitor interaction to guide further synthesis. Our idea that to select the lowest number of specific interactions within the allosteric site while maintaining a good affinity for the enzyme may be a valuable approach in overcoming drug resistance. A straightforward and versatile approach for the synthesis of new C6 arylmethyl functionalized S-DABOCs has been developed, leading to the identification of the lead compound **22a**. Biological results fully support our speculations about the possibility of selecting the lowest number of specific interactions within the NNIBP for the synthesis of novel NNRTIs able to overcome drug resistant mutations. In fact, **22a** was superior to both nevirapine and efavirenz in terms of relative resistance (that is, fold reduced activity, see Table 2), while in terms of absolute potencies it was similar to NVP and less potent than EFV. Exploitation of the above described synthetic procedure is underway in our laboratories to synthesize a large number of S-DABOC analogues hopefully endowed with an increased affinity for RT.

In a parallel study, a new class of NNRTIs with a 4-dimethylamino-6-vinylpyrimidine scaffold (DAVPs) has been identified and found to exhibit a peculiar behavior: contrary to the NNRTIs reported to date, enzymological studies reveal that such compounds inhibit HIV-1 RT by a competitive mechanism with the nucleotide substrate after binding to the NNIBP of the free enzyme. To the best of our knowledge, these compounds represent the first example of NNRTIs found to exhibit such behavior. The most active compound (**34a**) is characterized by a nanomolar activity ($K_i = 8$ nM) toward either the wild-type RT and common NNRTI-resistant mutants ($K_i = 12$ nM and 15 nM toward L100I and V179D, respectively). In contrast, K103N and Y181I mutations cause a marked decrease of the anti-RT activity up to the micro- and low micromolar range ($K_i = 3.2$ and 39 μM, respectively). The diethylamino analogue **34b** is about 2.5 orders of magnitude less active (although it retains a micromolar activity against the wild-type HIV-1), whereas the dibutyl analogue **34c** is almost inactive. These results suggest a significant sensitivity of this class of NNRTIs to the steric effects (that is, to the length of the alkyl substituents of the amino group). Enzymological studies reveal that DAVPs are nonclassical competitive inhibitors of RT with respect to the nucleotide substrate: the binding of these compounds to the allosteric site of the free RT enzyme may stabilize an open conformation of the catalytic site that, in the polymerization phase, does not allow for a proper binding of the incoming nucleotide. However, binding of the nucleotide substrate results in a closed conformation of RT that hinders the binding of the inhibitor.

Computational studies were carried out to rationalize the structure–activity relationships of DAVPs and to suggest a possible explanation for their unique mechanism of action. MM simulations allowed identification of the structural features responsible for the high activity of compound **34a** both on RT (wt) and selected NNRTI-resistant mutants (L100I and V179D), and to explain the other unsatisfactory biological results. MD simulations and superimposition analysis were finally performed on **34a**–RT complex in order to shed light on the competitive mechanism of action exerted by this inhibitor.

It was interesting to note that the binding of compound **34a** to the NNIBP determined a different pattern of conformational changes compared to that produced by common first- and second-generation NNRTIs: the side chain of Met 230 seemed to adopt an extended conformation whereas Asp 185 underwent a significant and peculiar shift, about 5.59 Å away from its original position and about 7.66 Å away from the position of the same residue in the TNK-651–RT complex. In particular, the unusual shift of Asp 185 could be ultimately responsible for the competitive mechanism of action exerted by the DAVPs as the magnesium ions in the catalytic site may lie so far apart, when **34a** is bound to the allosteric site, that no phosphodiester bond formation can take place. It was finally suggested that the major shift of this aspartate and the loss of the Gln 182–Met 184 hydrogen bond were involved in the disruption of the strained type II β-turn geometry around the RT active site. Further exploration of this new class of derivatives is still underway in our laboratories.

Experimental Section

General synthetic methods: All commercially available chemicals were used as purchased. CH_3CN was dried over calcium hydride, EtOH was dried over Mg/I_2, CH_2Cl_2 was dried over sodium hydride, and THF and dioxane were dried over Na/benzophenone prior to use whereas DMF was bought already anhydrous. Anhydrous reactions were run under a positive pressure of dry N_2 or argon. IR spectra were recorded on a Perkin-Elmer BX FTIR system, using KBr pellets. TLC was carried out using Merck TLC plates silica gel 60 F254. Chromatographic purifications were performed on columns packed with Merk 60 silica gel, 23–400 mesh, for flash technique. ^{1}H NMR and ^{13}C NMR spectra were recorded at 400 MHz on a Brucker Avance DPX400, at 300 MHz on a Varian VXR-300 and at 200 MHz on a Bruker AC200F spectrometer. Chemical shifts are reported relative to tetramethylsilane at 0.00 ppm. Elemental analyses (C, H, N) were performed in-house using a Perkin-Elmer Elemental Analyzer 240C. Melting points were taken using a Gallenkamp = melting point apparatus and are uncorrected. Mass spectra (MS) data were obtained using an Agilent 1100 LC/MSD VL system (G1946C) with a 0.4 mL min^{-1} flow rate using a binary solvent system of 95:5 methyl alcohol/water. UV detection was monitored at 254 nm. Mass spectra were acquired in positive and negative mode scanning over the mass range.

Compounds (**20a**, **22a**, **23**, **24**, **26b**, **27b**),[21] (**31**, **32b–d**, **33b–d**, **34b–d**)[23] and (**44a–c**, **45a–c**),[25] were prepared as already described.

Microwave irradiation experiments: Microwave irradiation experiments were conducted using a CEM Discover Synthesis Unit (CEM Corp., Matthews, NC). The machine consists of a continuous focused microwave power delivery system with operator-selectable power output from 0 to 300 W. The temperature of the reaction was monitored using a calibrated infrared temperature control mounted under the reaction vessel. All the experiments were performed using a stirring option whereby the contents of the vessel are stirred by means of rotating magnetic plate located below the floor of the microwave cavity and a Teflon-coated magnetic stir bar in the vessel.

Biological methods

Chemicals. [^{3}H] dTTP (40 Ci mmol^{-1}) was from Amersham and unlabeled dNTPs were from Boehringer. Whatman was the supplier of the GF/C filters. All other reagents were of analytical grade and purchased from Merck or Fluka.

Nucleic acid substrates. The homopolymer poly(rA) (Pharmacia) was mixed at weight ratios in nucleotides of 10:1, to the oligomer oligo(dT)12–18 (Pharmacia) in 20 mM Tris-HCl (pH 8.0), containing 20 mM KCl and 1 mM EDTA, heated at 65 °C for 5 min and then slowly cooled.

Expression and purification of recombinant HIV-1 RT forms. Recombinant heterodimeric wild-type RT, Leu100Ile, Val179Asp, Lys103Asn, and Tyr181Ile were expressed and purified to >95% purity (as judged by SDS-PAGE) as described.[15]

HIV-1 RT RNA-dependent DNA polymerase activity assay. RNA-dependent DNA polymerase activity was assayed as follows: a final volume of 25 μL contained buffer A (50 mM Tris-HCl pH 7.5, 1 mM DTT, 0.2 mg mL^{-1} BSA, 4% glycerol), 10 mM $MgCl_2$, 0.5 μg of poly(rA)/oligo(dT)10:1 (0.3 μM 3′-OH ends), 10 μM [^{3}H]dTTP (1 Ci mmol^{-1}), and 5–10 nM RT. Reactions were incubated for 10 min at 37 °C. 20 μL-Aliquots were then spotted on glass fiber filters GF/C which were immediately immersed in 5% ice-cold TCA. Filters were washed twice in 5% ice-cold TCA and, once in ethanol for 5 min, dried; the acid-precipitable radioactivity was measured by scintillation counting.

Inhibition assays. Reactions were performed under the conditions described for the HIV-1 RT RNA-dependent DNA polymerase activity assay. Incorporation of radioactive dTTP into poly(rA)/oligo(dT) at different concentrations of DNA or dNTP was monitored in the presence of increasing amounts of inhibitor as indicated in the figure legends. Data were analyzed according to the equation for a fully competitive inhibitor:

$$\nu = \frac{k_{cat}E_0}{1+\frac{K_m}{S}\left(1+\frac{I}{K_i}\right)} \quad (1)$$

Kinetics of inhibitor binding. Experiments were as described.[15] Briefly, HIV-1 RT (20–40 nM) was incubated 2 min at 37 °C in a final volume of 4 μL in the presence of buffer A, 10 mM $MgCl_2$ alone or with 100 nM 3′-OH ends (for the formation of the RT:TP complex) or in the same mixture complemented with 2 μM unlabeled dTTP (for the formation of the RT–T-dNTP complex). The inhibitor to be tested was then added to a final volume of 5 μL, at a concentration at which $[EI]/[E0] = (1-1/(1+[I]/K_i)) > 0.9$. Then, 145 μL of a mix containing buffer A, 10 mM $MgCl_2$ and 10 μM [^{3}H]dTTP (5 Ci mmol^{-1}) were added at different time points. After an additional 10 min of incubation at 37 °C, 50 μL aliquots were spotted on GF/C filters and acid-precipitable radioactivity measured as described for the HIV-1 RT RNA-dependent DNA polymerase activity assay. The quantity (v_t/v_0) representing the normalized difference between the amount of dTTP incorporated at the zero time point and at the different time points was then plotted against time. The k_{app} values were determined by fitting the experimental data to the single-exponential equation (Equation 2)

$$(v_t/v_0) = e^{-k}app^t \quad (2)$$

in which t is time. The K_{on} and K_{off} values were calculated according to the relationships :

$$k_{app} = k_{on}(K_i + [I]) \quad (3)$$

$$K_d = k_{off}/k_{on} \quad (4)$$

Computational methods

All molecular modeling calculations and manipulations were performed with the software packages MacroModel 8.5[45]/Maestro[46] and AutoDock 3.0,[36] running on SGI workstations. The united-atom Amber force field was used as implemented in MacroModel.

Docking studies. The structures of the compounds were built using the Maestro 3D-sketcher and fully minimized (Polak-Ribiere conjugate gradient, 0.05 kJ Å^{-1}mol convergence). Atom charges assigned to compounds during the minimization step were retained for the following docking calculations. For the docking procedure, the program AutoDock 3.0 was used to explore the binding conformation of S-DABOC and DAVPs on the wild-type and/or mutated RT. A grid spacing of 0.375 Å and 54×60×70 number of points was set, comprising all residues that constitute the NNRTI binding pocket. At each grid point, the receptor's atomic affinity potentials for carbon, oxygen, nitrogen, sulfur, and hydrogen were precalculated for rapid intra- and intermolecular energy evaluation of the docking solutions for each inhibitor. The genetic algorithm-local

search (GA-LS) method was used with the default settings and retrieved 100 docked conformations from each compound. Results from Autodock calculations were clustered with a RMSD tolerance of 1.5 Å and the lowest energy conformer of the most populated cluster (the lowest energy cluster in most cases) was selected as the most probable binding conformer. Ligand–HIV-1 complexes were submitted to a full minimization of the whole structure to a 0.1 KJ $Å^{-1}$ mol^{-1} gradient.

Molecular dynamics simulations. 34a–RT and **37b**–RT complexes were subjected to stochastic dynamics simulations. The united-atom Amber force field was used for all the simulations with the MacroModel 8.5. The complexes were restrained in the following manner: The protein residues that are within 21 Å of the mass center of the ligand, as well as the ligand, were allowed to move freely during the simulations. All the other residues were frozen to their positions. The SHAKE algorithm was applied for all the bonds involving hydrogen atoms. For the two complexes, 1000 ps stochastic dynamics simulations were carried out at 310 K with a time step of 2.0 fs, after an equilibration step of 100 ps. One hundred snapshots were collected. Minimizations and dynamics were carried out in aqueous solutions in all cases (not explicit).

Synthesis

2-(4′-methoxybenzylthio)-4-amino-5-methyl-6-(2,6-dichlorobenzyl)pyrimidine (4): Compound **3** (110 mg, 0.25 mmol) was dissolved in fresh distilled $POCl_3$ (2 mL) and the solution was heated at 105 °C for 1 h. After cooling to RT, water (10 mL) was added dropwise and the resulting solution neutralized by adding a saturated solution of $NaHCO_3$. The resulting mixture was diluted with ethyl acetate (30 mL), washed with brine (30 mL), dried over anhydrous Na_2SO_4, and evaporated to dryness under reduced pressure. In a sealed tube, the crude mixture was suspended in a methanolic solution of saturated ammonia (3 mL) and heated at 90 °C for 2 h. After cooling to room temperature the mixture was concentrated under reduced pressure and purified by flash chromatography on a silica gel column (eluent: ethyl acetate/petroleum ether 1:4) to give the desired product as a white solid (73 mg, 70%). R_f[ethyl acetate/petroleum ether 1:4] = 0.28; mp = 171–172 °C; ^{1}H NMR (200 MHz, CD_3OD): δ = 7.31 (d, J = 7.04 Hz, 2H), 7.13 (q, J = 8.88 Hz, 1H), 6.85 (t, J = 8.64 Hz, 2H), 6.67 (d, J = 6.69 Hz, 2H), 4.33 (s, 2H), 4.30 (bs, 2H), 3.87 (s, 2H), 3.71 (s, 3H), 2.13 ppm (s, 3H); MS (ESI): m/z 421 $[M+H]^+$, 443 $[M+Na]^+$; $C_{20}H_{19}Cl_2N_3OS$ Calcd: C, 57.15; H, 4.56; N, 10.00. Found: C, 57.21; H, 4.66; N, 10.09.

2-metiltio-6-[2-(*tert*-butyldimethylsyliloxy)ethyl]pyrimidin-4(3*H*)-one (6): TBDMSCl (300 mg, 2 mmol) and imidazole (136 mg, 2 mmol) were added to a solution of **5** (186 mg, 1 mmol) in dry DMF (3 mL), and the reaction mixture was stirred at RT for 1 h. The reaction mixture was then diluted with CH_2Cl_2 (20 mL), washed with water (3×10 mL) and brine (10 mL). The organic phase was dried over anhydrous Na_2SO_4 and evaporated to dryness under reduced pressure. Purification by flash chromatography on silica gel column (eluent: dichloromethane/methanol 99:1) gave the desired product **6** as a white solid (237 mg, 79%). R_f[dichloromethane/methanol 99:1] = 0.42; mp = 100–101 °C; IR ($CHCl_3$) $\tilde{\nu}$ = 1670 cm^{-1}; ^{1}H NMR (200 MHz, $CDCl_3$): δ = 6.60 (s, 1H), 3.91 (t, J = 6.33 Hz, 2H), 2.83 (t, J = 6.42 Hz, 2H), 2.43 (s, 3H), 0.80 (s; 9H), 0.05 ppm (s, 6H), MS (ESI): m/z 301 $[M+H]^+$, 323 $[M+Na]^+$; Anal for $C_{13}H_{24}N_2O_2SSi$ Calcd: C, 51.96; H, 8.05; N, 9.32. Found: C, 52.15; H, 8.31; N, 9.58.

2-methylthio-4-chloro-6-[2-(*tert*-butyldimethylsyliloxy)ethyl]pyrimidine (7): A solution of $SOCl_2$ (80 μL, 1.1 mmol) in dry DMF (1 mL) was added dropwise to a solution of **6** (300 mg, 1 mmol) in dry CH_2Cl_2 (5 mL). The reaction mixture was stirred at RT for 40 min and then quenched by carefully adding a saturated solution of $NaHCO_3$ (10 mL). The organic phase was washed with water (3× 10 mL) and brine (10 mL), dried over anhydrous Na_2SO_4, and evaporated to dryness under reduced pressure. The product was purified by flash chromatography on silica gel column (eluent: ethyl acetate/petroleum ether 1:8) to give the desired product **7** as a white solid (222 mg, 70%). R_f[ethyl acetate/petroleum ether 1:8] = 0.48; mp = 121–122 °C; ^{1}H NMR (200 MHz, $CDCl_3$): δ = 7.02 (s, 1H), 3.95 (t, J = 5.55 Hz, 2H), 2.89 (t, J = 5.36 Hz, 2H), 2.50 (s, 3H), 0.82 (s, 9H), 0.05 (s, 6H); MS (ESI): m/z 320 $[M+H]^+$, Anal for $C_{13}H_{23}ClN_2OSSi$ Calcd: C, 48.96; H, 7.27; N, 8.78. Found: C, 48.90; H, 7.39; N, 8.86.

2-methylthio-4-chloro-6-(2-hydroxyethyl)pyrimidine (8): Tetrabutylammonium fluoride (2.50 mL, 1 M in THF, 2.50 mmol) was added to a solution of **7** (200 mg, 0.63 mmol) in dry THF (5 mL) and the solution was stirred at RT for 1 h. The reaction mixture was concentrated under reduced pressure and the crude product was purified by flash chromatography on silica gel column (eluent: ethyl acetate/petroleum ether 1:1) to give the desired alcohol **8** as a white solid (113 mg, 88%). R_f[ethyl acetate/petroleum ether 1:1] = 0.40; mp = 91–92 °C; IR ($CHCl_3$) $\tilde{\nu}$ = 3381 cm^{-1}; ^{1}H NMR (200 MHz, $CDCl_3$): δ = 6.88 (s, 1H), 3.99 (t, J = 5.52 Hz, 2H), 2.90 (t, J = 5.31 Hz, 2H), 2.53 ppm (s, 3H); MS (ESI): m/z 205 $[M+H]^+$, Anal for $C_7H_9ClN_2OS$ Calcd: C, 41.08; H, 4.43; N, 13.69. Found: C, 41.30; H, 4.56; N, 13.88.

2-methylthio-4-amino-6-(2-hydroxyethyl)pyrimidine (9): In a sealed tube, compound **8** (46 mg, 0.25 mmol) was suspended in a methanolic solution of saturated ammonia (2 mL) and heated at 90 °C for 3 h. After cooling to RT the mixture was concentrated under reduced pressure and purified by flash chromatography on a silica gel column (eluent: dichloromethane/methanol 97:3) to give the desired product as a white solid (14 mg, 30%). R_f[dichloromethane/methanol 97:3] = 0.31; mp = 99–100 °C; IR ($CHCl_3$) $\tilde{\nu}$ = 3532, 3428, 3315 cm^{-1}; ^{1}H NMR (200 MHz, $CDCl_3$): δ = 6.14 (s, 1H), 5.20 (bs, 2H), 3.79 (t, J = 6.25 Hz, 2H), 2.67 (t, J = 6.23 Hz, 2H), 2.48 ppm (s, 3H); MS (ESI): m/z 186 $[M+H]^+$; Anal for $C_7H_{11}N_3OS$ Calcd: C, 45.39; H, 5.99; N, 22.68. Found: C, 45.60; H, 6.22; N, 22.81.

2-methylthio-4-amino-6-vinylpyrimidine (10): NaH (72 mg, 3 mmol) was added to a solution of **9** (168 mg, 1 mmol) in dry dioxane (5 mL), and the resulting suspension was heated to reflux for 3 h. After cooling to RT the reaction was quenched by slow addition of water. The crude mixture was diluted with ethyl acetate (20 mL), washed with water (20 mL) and brine (20 mL), dried over anhydrous Na_2SO_4, and evaporated to dryness under reduced pressure. The product was purified by flash chromatography on silica gel column (eluent: dichloromethane/methanol 96:4) to give the desired amine **10** as a white solid (118 mg, 71%). R_f[dichloromethane/methanol 96:4] = 0.66; mp = 63–64 °C; IR ($CHCl_3$) $\tilde{\nu}$) = 3516, 3436 cm^{-1}; ^{1}H NMR (200 MHz, $CDCl_3$): δ = 7.11 (dd, J_{trans} = 17.09 Hz, J_{cis} = 10.03 Hz, 1H), 6.01 (s, 1H), 6.54 (dd, J_{trans} = 16.70 Hz, J_{gem} = 2.00 Hz, 1H), (dd, J_{cis} = 10.03 Hz, J_{gem} = 1.98 Hz, 1H), 5.02 (bs, 2H), 2.50 ppm (s, 3H); MS (ESI): m/z 168 $[M+H]^+$; Anal for $C_7H_9N_3S$ Calcd: C, 50.27; H, 5.42; N, 25.13. Found: C, 50.51; H, 5.70; N, 25.31.

General procedure for the synthesis of (13) and (14): Sodium (0.611 g; 26.56 mmol) was dissolved in absolute ethanol (40 mL) under a positive pressure of dry N_2. Thiourea (1.41 g; 18.58 mmol) and the appropriate β-ketoester (**11**; **12**) (13.27 mmol) were added to the clear solution and the reaction mixture was heated to 80 °C

for 12 h. After cooling to RT the mixture was concentrated under reduced pressure, the crude residue was dissolved in water (20 mL), and neutralized by adding CH_3COOH 0.5 N. The aqueous phase was extracted with ethyl acetate (3×25 mL) and the combined organic layers were washed with brine (20 mL), dried over anhydrous Na_2SO_4, and evaporated to dryness under reduced pressure. The products were recrystallized from ethanol.

6-(4-fluorobenzyl)-2,3-dihydro-2-thioxopyrimidin-4(1*H*)-one (13): White solid, 2.22 g (71%); R_f[ethyl acetate/petroleum ether 1:1] = 0.35; mp = 225–227 °C; IR (nujol) $\tilde{\nu}$ = 1682 cm^{-1}; ^1H NMR (200 MHz, $CDCl_3$): δ = 7.30 (q, J = 8.37 Hz, 2H), 7.14 (t, J = 8.50 Hz, 2H), 5.49 (s, 1H), 3.72 ppm (s, 2H); MS (ESI): *m/z* 237 $[M+H]^+$; Anal for $C_{11}H_9FN_2OS$ Calcd: C, 55.92; H, 3.84; N, 11.86. Found: C, 56.12; H, 4.01; N, 11.52.

6-(4-fluorobenzyl)-2,3-dihydro-5-methyl-2-thioxopyrimidin-4-(1H)-one (14): White solid; 2.22 g (67%); R_f[ethyl acetate/petroleum ether 1:1] = 0.41; mp = 242–244 °C; IR (nujol) $\tilde{\nu}$ = 1682 cm^{-1}; ^1H NMR (200 MHz, $CDCl_3$): δ = 7.09 (q, J = 8.44 Hz, 2H), 6.95 (t, J = 8.75 Hz, 2H), 3.75 (s, 2H), 1.86 ppm (s, 3H); MS (ESI): *m/z* 273 $[M+Na]^+$; Anal for $C_{12}H_{11}FN_2OS$ Calcd: C, 57.58; H, 4.43; N, 11.19. Found: C, 57.63; H, 4.82; N, 11.42.

General procedure for the synthesis of (15a–c) and (16a–c): The appropriate alkyl halide (0.4 mmol) (Methyl iodide for **15a**, **16a**, ethyl bromide for **15b**, **16b** and propyl bromide for **15c**, **16c**) was added to a solution of the appropriate thiopyrimidine (**13**; **14**) (0.2 mmol) in dry DMF (2 mL) and the reaction mixture was irradiated at 130 °C for 5 min. After cooling to RT the suspension was diluted with ethyl acetate (10 mL) and then washed with water (2× 15 mL) and brine (15 mL). The organic phase was dried over anhydrous Na_2SO_4 and evaporated under reduced pressure. The crude residue was purified by flash chromatography on silica gel column (eluent: ethyl acetate/petroleum ether 1:1 for **15a–c** and dichloromethane/methanol 96:4 for **16a–c**) to give the desired product.

2-Methylthio-6-(4-fluorobenzyl)-4(3H) pyrimidinone (15a): Pink solid (30 mg, 61%); R_f[ethyl acetate/petroleum ether 1:1] = 0.33; mp = 163–164 °C; IR (nujol) $\tilde{\nu}$ = 1650 cm^{-1}; ^1H NMR (200 MHz, $CDCl_3$): δ = 7.28 (q, J = 8.67 Hz, 2H), 7.01 (t, J = 9.00 Hz, 2H), 5.89 (s, 1H), 3.79 (s, 2H), 2.51 (s, 3H); MS (ESI): *m/z* 273 $[M+Na]^+$; Anal for $C_{12}H_{11}FN_2OS$ Calcd: C, 57.58; H, 4.43; N, 11.19. Found: C, 57.72; H, 4.23; N, 10.98.

2-Ethylthio-6-(4-fluorobenzyl)-4(3H) pyrimidinone (15b): White solid (72 mg, 80%); R_f[ethyl acetate/petroleum ether 1:1] = 0.40; mp = 167–168 °C; IR (nujol) $\tilde{\nu}$ = 1655 cm^{-1} (C=O); ^1H NMR (200 MHz, $CDCl_3$): δ = 7.20 (q, J = 8.54 Hz, 2H), 6.96 (t, J = 8.43 Hz, 2H), 5.81 (s, 1H), 3.82 (s, 2H), 3.00 (q, J = 7.44 Hz, 2H), 1.24 ppm (t, J = 7.38 Hz, 3H); MS (ESI): *m/z* 265 $[M+H^+]$, 287 $[M+Na]^+$; Anal for $C_{13}H_{13}FN_2OS$ Calcd: C, 59.07; H, 4.96; N, 10.60. Found: C, 59.10; H, 5.13; N, 10.45.

2-Propylthio-6-(4-fluorobenzyl)-4(3H) pyrimidinone (15c): White solid (42 mg, 75%); mp = 170–171 °C; R_f [ethyl acetate/petroleum ether 1:1] = 0.50; IR (nujol) $\tilde{\nu}$ = 1653; ^1H NMR (200 MHz, $CDCl_3$): δ = 7.22 (q, J = 8.77 Hz, 2H), 6.99 (t, J = 8.44 Hz, 2H), 5.85 (s, 1H), 3.80 (s, 2H), 3.03 (t, J = 6.85 Hz, 2H), 1.62 (m, 2H), 0.95 (t, J = 7.15 Hz, 3H); MS (ESI): *m/z* 279 $[M+H]^+$, 301 $[M+Na]^+$, 317 $[M+K]^+$; Anal for $C_{14}H_{15}FN_2OS$ Calcd: C, 60.41; H, 5.43; N, 10.06. Found: C, 60.58; H, 5.34; N, 10.21.

2-Methylthio-5-methyl-6-(4-fluorobenzyl)-4(3H) pyrimidinone (16a): White solid (38 mg, 68%); R_f[dichloromethane/methanol 96:4] = 0.24; mp = 184–185 °C; IR (nujol) $\tilde{\nu}$ = 1650 cm^{-1}; ^1H NMR (200 MHz, $CDCl_3$): δ = 7.24 (q, J = 8.70 Hz, 2H), 6.97 (t, J = 8.94 Hz, 2H), 3.89 (s, 2H), 2.46 (s, 3H), 1.99 ppm (s, 3H); MS (ESI): *m/z* 265 $[M+H]^+$, 287 $[M+Na]^+$, Anal for $C_{13}H_{13}FN_2OS$ Calcd: C, 59.07; H, 4.96; N, 10.60. Found: C, 60.23; H, 5.21; N, 10.31.

2-Ethylthio-5-methyl-6-(4-fluorobenzyl)-4(3H) pyrimidinone (16b): White solid (50 mg, 90%); R_f[dichloromethane/methanol 96:4] = 0.30; mp = 167 °C; IR (nujol) $\tilde{\nu}$ = 1650 cm^{-1}; ^1H NMR (200 MHz, $CDCl_3$): δ = 7.19 (q, J = 8.66 Hz, 2H), 6.94 (t, J = 8.53 Hz, 2H), 3.84 (s, 2H), 3.06 (q, J = 7.38 Hz, 2H), 2.07 (s, 3H), 1.25 ppm (t, J = 7.33 Hz, 3H); MS (ESI): *m/z* 279 $[M+H^+]$, 301 $[M+Na]^+$; Anal for $C_{14}H_{15}FN_2OS$ Calcd: C, 60.41; H, 5.43; N, 10.06. Found: C, 60.62; H, 5.30; N, 10.35.

2-Propylthio-5-methyl-6-(4-fluorobenzyl)-4(3H) pyrimidinone (16c): White solid; (50 mg, 85%); R_f[dichloromethane/methanol 96:4] = 0.38; mp = 147–148 °C; IR (nujol) $\tilde{\nu}$ = 1638 cm^{-1}; ^1H NMR (200 MHz, $CDCl_3$): δ = 7.18 (q, J = 8.62 Hz, 2H), 6.94 (t, J = 8.50 Hz, 2H), 3.84 (s, 2H), 3.02 (t, J = 6.85 Hz, 2H), 2.08 (s, 3H), 1.62 (m, 2H), 0.93 ppm (t, J = 7.15 Hz, 3H); MS (ESI): *m/z* 293 $[M+H]^+$, 315 $[M+Na]^+$, 331 $[M+K]^+$; Anal for $C_{15}H_{17}FN_2OS$ Calcd: C, 61.62; H, 5.86; N, 9.58. Found: C, 61.40; H, 5.75; N, 9.74.

General procedure for the synthesis of (19a–c) and (20a–c): $SOCl_2$ was added (6 mmol) to a solution of the appropriate thiopyrimidinone (**15a–c**; **16a–c**) (1 mmol) in dry DMF (5 mL) and the reaction mixture was stirred at RT for 36 h. Then water (15 mL) was added and the suspension was heated under reflux for 12 h. After cooling to RT the mixture was diluted with ethyl acetate (20 mL) and then washed with water (15 mL) and brine (15 mL). The organic phase was dried over anhydrous Na_2SO_4 and evaporated under reduced pressure. The crude residue was purified by flash chromatography on silica gel column (eluent: petroleum ether/diethyl ether 9:1 for **19a–c** and petroleum ether/diethyl ether 99:1 for **20a–c**) to give the desired compound.

2-Methylthio-4-chloro-6-(4-fluorobenzoyl)pyrimidine (19a): White solid (121 mg, 43%); R_f[petroleum ether/diethyl ether 9:1] = 0.35; mp = 100–101 °C; IR ($CHCl_3$) $\tilde{\nu}$ = 1672 cm^{-1}; ^1H NMR (200 MHz, $CDCl_3$): δ = 8.15 (q, J = 8.85 Hz, 2H), 7.58 (s, 1H), 7.25 (t, J = 8.78 Hz, 2H), 2.54 ppm (s, 3H); MS (ESI): *m/z* 283 $[M+H]^+$; Anal for $C_{12}H_8ClFN_2OS$ Calcd: C, 50.98; H, 2.85; N, 9.91. Found: C, 51.02; H, 2.93; N, 10.15.

2-Ethylthio-4-chloro-6-(4-fluorobenzoyl)pyrimidine (19b): White solid (148 mg, 50%); R_f[petroleum ether/diethyl ether 9:1] = 0.38; mp = 105 °C; IR ($CHCl_3$) $\tilde{\nu}$ = 1675 cm^{-1}; ^1H NMR (200 MHz, $CDCl_3$): δ = 8.14 (q, J = 8.77 Hz, 2H), 7.55 (s, 1H), 7.20 (t, J = 8.67 Hz, 2H), 2.71 (q, J = 7.40 Hz, 2H), 1.28 ppm (t, J = 7.39 Hz, 3H); MS (ESI): *m/z* 297 $[M+H]^+$; Anal for $C_{13}H_{10}ClFN_2OS$ Calcd: C, 52.62; H, 3.40; N, 9.44. Found: C, 52.72; H, 3.48; N, 9.60.

2-Propylthio-4-chloro-6-(4-fluorobenzoyl)pyrimidine (19c): White solid; (124 mg, 40%); R_f[petroleum ether/diethyl ether 9:1] = 0.45; mp = 110–111 °C; IR ($CHCl_3$) $\tilde{\nu}$ = 1675 cm^{-1}; ^1H NMR (200 MHz, $CDCl_3$): δ = 8.15 (q, J = 8.69 Hz, 2H), 7.51 (s, 1H), 7.23 (t, J = 8.61 Hz, 2H), 3.03 (t, J = 6.85 Hz, 2H), 1.62 (m, 2H), 0.95 ppm (t, J = 7.15 Hz, 3H); MS (ESI): *m/z* 311 $[M+H]^+$; Anal for $C_{14}H_{12}ClFN_2OS$ Calcd: C, 54.11; H, 3.89; N, 9.01. Found: C, 54.22; H, 3.98; N, 9.15.

2-Methylthio-4-chloro-5-methyl-6-(4-fluorobenzoyl)pyrimidine (20a): White solid (103 mg, 35%); R_f[petroleum ether/diethyl ether 99:1] = 0.46; mp = 101–102 °C; IR ($CHCl_3$) $\tilde{\nu}$ = 1673 cm^{-1}; ^1H NMR (200 MHz, $CDCl_3$): δ = 7.87 (q, J = 8.55 Hz, 2H), 7.15 (t, J = 8.51 Hz, 2H), 2.50 (s, 3H), 2.23 ppm (s, 3H); MS (ESI): *m/z* 319 $[M+Na]^+$, 335 $[M+K]^+$; Anal for $C_{13}H_{10}ClFN_2OS$ Calcd: C, 52.62; H, 3.40; N, 9.44. Found: C, 52.81; H, 3.56; N, 9.18.

2-Ethylthio-4-chloro-5-methyl-6-(4-fluorobenzoyl)pyrimidine (20 b): White solid (102 mg, 33%); R_f[petroleum ether/diethyl ether 99:1] = 0.49; Mp = 103–104 °C; IR ($CHCl_3$) $\tilde{\nu}$ = 1670 cm^{-1}; ^1H NMR (200 MHz, $CDCl_3$): δ = 7.87 (q, J = 8.69 Hz, 2H), 7.17 (t, J = 8.49 Hz, 2H), 3.07 (q, J = 6.92 Hz, 2H), 2.21 (s, 3H), 1.32 ppm (t, J = 7.05 Hz, 3H); MS (ESI): m/z 311 $[M+H]^+$, 333 $[M+Na]^+$; Anal for $C_{14}H_{12}ClFN_2OS$ Calcd: C, 54.11; H, 3.89; N, 9.01. Found: C, 54.22; H, 3.70; N, 9.10.

2-Propylthio-4-chloro-5-methyl-6-(4-fluorobenzoyl)pyrimidine (20 c): White solid (113 mg, 35%); R_f [petroleum ether/diethyl ether 99:1] = 0.55; mp = 72–73 °C; IR ($CHCl_3$) $\tilde{\nu}$ = 1681 cm^{-1}; ^1H NMR (200 MHz, $CDCl_3$): δ = 7.95 (q, J = 8.70 Hz, 2H), 7.20 (t, J = 8.45 Hz, 2H), 3.15 (t, J = 6.60 Hz, 2H), 2.23 (s, 3H), 1.63 (m, 2H), 0.95 ppm (t, J = 6.51 Hz, 3H); MS (ESI): m/z 325 $[M+H]^+$, 347 $[M+Na]^+$; Anal for $C_{15}H_{14}ClFN_2OS$ Calcd: C, 55.47; H, 4.34; N, 8.62. Found: C, 55.57; H, 4.38; N, 8.74.

General procedure for the synthesis of (21 a–c) and (22 a–c): In a sealed tube, the appropriate substrate (0.25 mmol) was suspended in a methanolic solution of saturated ammonia (2 mL) and heated at 90 °C for 2 h. After cooling to room temperature the mixture was concentrated under reduced pressure and purified by flash chromatography on a silica gel column (eluent: dichloromethane/methanol 98:2) to give the desired product.

2-Methylthio-6-(4-fluorobenzoyl)cytosine (21 a): White solid (52 mg, 80%); R_f[dichloromethane/methanol 98:2] = 0.33; mp = 197–198 °C; IR ($CHCl_3$) $\tilde{\nu}$ = 3533, 3421, 1668 cm^{-1}; ^1H NMR (200 MHz, $CDCl_3$): δ = 8.19 (q, J = 8.88 Hz, 2H), 7.14 (t, J = 8.80 Hz, 2H), 6.67 (s, 1H), 5.08 (bs, 2H), 2.47 ppm (s, 3H); MS (ESI): m/z 264 $[M+H]^+$; Anal for $C_{12}H_{10}FN_3OS$ Calcd: C, 54.74; H, 3.83; N, 15.96. Found: C, 54.84; H, 3.92; N, 15.79.

2-Ethylthio-6-(4-fluorobenzoyl)cytosine (21 b): White solid (55 mg, 80%); R_f[dichloromethane/methanol 98:2] = 0.40; mp = 188 °C; IR ($CHCl_3$) $\tilde{\nu}$ = 3530, 3425, 1665 cm^{-1}; ^1H NMR (200 MHz, $CDCl_3$): δ = 8.15 (q, J = 8.95 Hz, 2H), 7.17 (t, J = 8.78 Hz, 2H), 6.65 (s, 1H), 5.10 (bs, 2H), 2.55 (q, J = 7.22 Hz, 2H), 1.21 ppm (t, J = 7.47 Hz, 3H); MS (ESI): m/z 278 $[M+H]^+$; Anal for $C_{13}H_{12}FN_3OS$ Calcd: C, 56.30; H, 4.36; N, 15.15. Found: C, 56.41; H, 4.49; N, 15.19.

2-Propylthio-6-(4-fluorobenzoyl)cytosine (21 c): White solid (62 mg, 86%); R_f[dichloromethane/methanol 98:2] = 0.41; mp = 174–175 °C; IR ($CHCl_3$) $\tilde{\nu}$ = 3527, 3430, 1670 cm^{-1}; ^1H NMR (200 MHz, $CDCl_3$): δ = 8.11 (q, J = 8.94 Hz, 2H), 7.12 (t, J = 8.80 Hz, 2H), 6.55 (s, 1H), 5.13 (bs, 2H), 3.29 (t, J = 6.99 Hz, 2H), 1.58 (m, 2H), 0.93 ppm (t, J = 7.07 Hz, 3H); MS (ESI): m/z 292 $[M+H]^+$; Anal for $C_{14}H_{14}FN_3OS$ Calcd: C, 57.72; H, 4.84; N, 14.42. Found: C, 57.81; H, 4.74; N, 14.53.

2-Ethylthio-5-methyl-6-(4-fluorobenzoyl)cytosine (22 b): White solid (51 mg, 70%); R_f[dichloromethane/methanol 98:2] = 0.51; mp = 192–193 °C; IR ($CHCl_3$) $\tilde{\nu}$ = 3518, 3430, 1666 cm^{-1}; ^1H NMR (400 MHz, $CDCl_3$): δ = 7.93 (q, J = 8.47 Hz, 2H), 7.12 (t, J = 8.33 Hz, 2H), 5.27 (bs, 2H), 3.02 (q, J = 7.67 Hz, 2H), 2.00 (s, 3H), 1.28 ppm (t, J = 7.05 Hz, 3H); MS (ESI): m/z 292 $[M+H]^+$; Anal for $C_{14}H_{14}FN_3OS$ Calcd: C, 57.72; H, 4.84; N, 14.42. Found: C, 57.90; H, 4.90; N, 14.31.

2-Propylthio-5-methyl-6-(4-fluorobenzoyl)cytosine (22 c): White solid (57 mg, 75%); R_f[dichloromethane/methanol 98:2] = 0.63; mp = 190–191 °C; IR ($CHCl_3$) $\tilde{\nu}$ = 3515, 3425, 1669 cm^{-1}; ^1H NMR (400 MHz, $CDCl_3$): δ = 7.93 (q, J = 8.61 Hz, 2H), 7.11 (t, J = 8.52 Hz, 2H), 4.98 (bs, 2H), 2.97 (t, J = 7.04 Hz, 2H), 1.98 (s, 3H), 1.63 (m, 2H), 0.92 ppm (t, J = 7.70, 3H); MS (ESI): m/z 306 $[M+H]^+$; Anal for $C_{15}H_{16}FN_3OS$ Calcd: C, 59.00; H, 5.28; N, 13.76. Found: C, 59.12; H, 5.35; N, 13.83.

2-Methylthio-5-methyl-6-(4-fluorobenzoyl)cytosine (25 c): K_2CO_3 (100 mg, 0.72 mmol) was added to a solution of **20 a** (70 mg; 0.24 mmol) in $HNMe_2$ (2 mL, 2 M in THF, large excess) and the mixture was stirred at RT for 1 h. The suspension was diluted with ethyl acetate (20 mL) and washed with brine (15 mL). The organic phase was dried over anhydrous Na_2SO_4 and evaporated to dryness under reduced pressure. The crude product was purified by flash chromatography on silica gel column (eluent: ethyl acetate/petroleum ether 1:9) to give the desired product as a white solid (61 mg, 83%). R_f[ethyl acetate/petroleum ether 1:9] = 0.55; mp = 85 °C; IR ($CHCl_3$) $\tilde{\nu}$ = 1678 cm^{-1}; ^1H NMR (200 MHz, $CDCl_3$): δ = 7.86 (q, J = 7.83 Hz, 2H), 7.05 (t, J = 8.44 Hz, 2H), 3.04 (s, 6H), 2.41 (s, 3H), 2.05 ppm (s, 3H); ^{13}C NMR (200 MHz, $CDCl_3$) δ = 193.26, 167.40, 165.36, 164.96, 162.22, 133.02, 131.82, 115.84, 108.26, 40.49, 15.41, 14.05 ppm; MS (ESI): m/z 306 $[M+H]^+$, 328 $[M+Na]^+$; Anal for $C_{15}H_{16}FN_3OS$ Calcd: C, 59.00; H, 5.28; N, 13.76 Found: C, 59.13; H, 5.40; N, 13.87.

General procedure for the synthesis of compounds (26 c) and (29): The appropriate substrate (**25 c** or **28**, 0.30 mmol) was dissolved in dry THF (6 mL) under argon atmosphere. The solution was cooled to −15 °C then methylmagnesium bromide (0.60 mmol, 3 M in Et_2O) was added dropwise. The reaction was brought to RT, stirred for 1 h and then quenched by adding a saturated solution of NH_4Cl (30 mL). The crude mixture was diluted with ethyl acetate (30 mL) and then washed with brine (30 mL), dried over anhydrous Na_2SO_4, and evaporated to dryness under reduced pressure. The crude product was purified by flash chromatography on silica gel column (eluent: ethyl acetate/petroleum ether 1:9 for **26 c** and ethyl acetate/petroleum ether 1:3 for **29**) to give the desired product.

2-methylthio-4-dimethylamino-5-methyl-6-[1-(4-fluorophenyl)-1-(hydroxyl)ethyl]pyrimidine (26 c): Yellow oil (67 mg, 70%); R_f [ethyl acetate/petroleum ether 1:9] = 0.22; IR ($CHCl_3$) $\tilde{\nu}$ = 3307 cm^{-1}; ^1H NMR (200 MHz, $CDCl_3$): δ = 7.23 (q, J = 8.38 Hz, 2H), 6.90 (t, J = 8.53 Hz, 2H), 2.87 (s, 6H), 2.50 (s, 3H), 1.82 (s, 3H),1.60 ppm (s, 3H); ^{13}C NMR (200 MHz, $CDCl_3$) δ = 169.06, 167.72, 165.12, 163.16, 141.19, 128.30, 115.03, 107.93, 74.02, 41.04, 29.70, 26.07, 15.51 ppm; MS (ESI): m/z 322 $[M+H]^+$, 344 $[M+Na]^+$; $C_{16}H_{20}FN_3OS$ Calcd: C, 59.79; H, 6.27; N, 13.07 Found: C, 59.88; H, 6.33; N, 13.15.

2-methylthio-4-dimethylamino-5-methyl-6-[1-(4-dimethylamino-phenyl)-1-(hydroxyl)ethyl]pyrimidine (29): Colorless oil; (98 mg, 95%); R_f [ethyl acetate/petroleum ether 1:3] = 0.40; IR ($CHCl_3$) $\tilde{\nu}$ = 3325 cm^{-1}; ^1H NMR (200 MHz, $CDCl_3$): δ = 7.15 (d, J = 8.80 Hz, 2H), 6.63 (d, J = 8.79 Hz, 2H), 2.91 (s, 6H), 2.89 (s, 6H), 2.55 (s, 3H), 1.85 (s, 3H), 1.71 ppm (s, 3H); ^{13}C NMR (200 MHz, $CDCl_3$) δ = 169.07, 167.69, 165.11, 149.67, 133.09, 127.13, 112.24, 108.32, 74.08, 40.98, 40.50, 28.63, 15.44, 14.00 ppm; MS (ESI): m/z 347 $[M+H]^+$; 369 $[M+Na]^+$, 715 $[2M+Na]^+$; $C_{18}H_{26}N_4OS$ Calcd: C, 62.40; H, 7.56; N, 16.17 Found: C, 62.48; H, 7.60; N, 16.25.

General procedure for the synthesis of compounds (27 c) and (30): To a suspension of the appropriate substrate (**26 c** and **29**, 0.30 mmol) in dry Et_2O (5 mL) 2,6-lutidine (0.48 mmol) was added at −5 °C. After stirring for 5 min at the same temperature $(CF_3CO)_2O$ was added (0.45 mmol) and the reaction mixture was stirred for 1 h at RT. The suspension was diluted with Et_2O, washed with a solution of HCl 1 N (10 mL), water (15 mL) and brine (15 mL). The organic layer was dried over anhydrous Na_2SO_4 and evaporated to dryness under reduced pressure. The crude mixture was suspended in glacial acetic acid and heated at 60 °C for 30 min. After

cooling to RT the mixture was diluted with EtOAc and neutralized by adding a saturated solution of Na_2CO_3. The organic phase was washed with water (20 mL) and brine (20 mL), dried over anhydrous Na_2SO_4, and evaporated to dryness under reduced pressure. The crude product was purified by flash chromatography on silica gel column (eluent: ethyl acetate/petroleum ether 1:6 for **27c** and ethyl acetate/petroleum ether 1:3 for **30**).

2-methylthio-4-dimethylamino-5-methyl-6-[1-(4-fluorophenyl)vinyl]cytosine (27c): Colorless oil (73 mg, 80%); R_f[ethyl acetate/petroleum ether 1:6] = 0.57; ^{1}H NMR (200 MHz, $CDCl_3$): δ = 7.27 (q, J = 8.74 Hz, 2H), 6.94 (t, J = 8.84 Hz, 2H), 5.77 (s, 1H), 5.38 (s, 1H), 3.01 (s, 6H), 2.50 (s, 3H), 1.91 ppm (s, 3H); ^{13}C NMR (200 MHz, $CDCl_3$) δ = 167.04, 166.24, 166.13, 163.73, 161.28, 146.44, 134.94, 128.13, 116.90, 115.22, 109.16, 40.61, 16.49, 14.06 ppm, MS (ESI): m/z 304 $[M+H]^+$, 326 $[M+Na]^+$; $C_{16}H_{18}FN_3S$ Calcd: C, 63.34; H, 5.98; N, 13.85 Found: C, 63.40; H, 6.10; N, 13.93.

2-methylthio-4-dimethylamino-5-methyl-6-[1-(4-dimethylaminophenyl)vinyl]cytosine (30): Colorless oil (87 mg, 89%); R_f[ethyl acetate/petroleum ether 1:3] = 0.55; ^{1}H NMR (200 MHz, $CDCl_3$): δ = 7.18 (d, J = 8.79 Hz, 2H), 6.62 (d, J = 8.82 Hz, 2H), 5.68 (s, 1H), 5.17 (s, 1H), 3.00 (s, 6H), 2.93 (s, 6H), 2.51 (s, 3H), 1.93 ppm (s, 3H); ^{13}C NMR (200 MHz, $CDCl_3$) δ = 167.92, 166.76, 166.12, 150.13, 147.12, 127.28, 126.80, 112.77, 112.07, 109.52, 40.65, 40.38, 16.33, 14.08 ppm; MS (ESI): m/z 329 $[M+H]^+$; $C_{18}H_{24}N_4S$ Calcd: C, 65.82; H, 7.36; N, 17.06 Found: C, 65.88; H, 7.44; N, 17.12.

2-Methylthio-4-dimethylamino-5-methyl-6-(4-dimethylaminobenzoyl)pyrimidine (28): Dimethylamine (255 μL, 0.51 mmol, 2 M in THF) and K_2CO_3 (54 mg, 0.51 mmol) were added to a solution of **24** (37 mg, 0.08 mmol) in dry DMF (2 mL). The reaction mixture was irradiated in a microwave oven at 90 °C for 10 min. After cooling to RT the suspension was diluted with EtOAc (10 mL) and then washed with water (15 mL) and brine (15 mL). The organic phase was dried over anhydrous Na_2SO_4 and evaporated under reduced pressure. The crude residue was purified by flash chromatography on silica gel column (eluent: Ethyl acetate/petroleum ether 1:3) to give the desired product as a white solid (21 mg, 82%). R_f[ethyl acetate/petroleum ether 1:3] = 0.28; mp = 197 °C; IR ($CHCl_3$) $\tilde{\nu}$ = 1650 cm^{-1}; ^{1}H NMR (200 MHz, $CDCl_3$): δ = 7.73 (d, J = 9.07 Hz, 2H), 6.60 (d, J = 8.93 Hz, 2H), 3.06 (s, 6H), 3.04 (s, 6H), 2.47 (s, 3H), 2.07 ppm (s, 3H); ^{13}C NMR (200 MHz, $CDCl_3$) δ = 192.82, 166.99, 165.28, 164.07, 153.90, 132.91, 123.12, 110.60, 107.86, 40.41, 39.89, 15.23, 13.96 ppm; MS: m/z 331 $[M+H]^+$; 353 $[M+Na]^+$; 683 $[2M+Na]^+$, $C_{17}H_{22}N_4OS$ Calcd: C, 61.79; H, 6.71; N, 16.95 Found: C, 61.85; H, 6.80; N, 16.89.

General procedure for the synthesis of compounds 32a–d, 33a–d, 34a–d: (see Ref. [23]).

2-methylthio-4-dimethylamino-6-(2-hydroxyethyl)pyrimidine (32a): White solid (320 mg, 83%). R_f[ethyl acetate/petroleum ether 2:1] = 0.20; mp = 86.5–87.8 °C (crystallized from AcOEt); IR ($CHCl_3$) $\tilde{\nu}$ = 3387 cm^{-1}; ^{1}H NMR (200 MHz, $CDCl_3$): δ = 5.94 (s, 1H), 4.36 (bs, 1H), 3.91 (t, J = 5.38 Hz, 2H), 3.07 (s, 6H), 2.74 (t, J = 5.38 Hz, 2H), 2.46 ppm (s, 3H); MS (ESI): m/z 214 $[M+H]^+$, 236 $[M+Na]^+$, 449 $[2M+Na]^+$. Anal. for $C_9H_{15}N_3OS$ Calcd: C, 50.68; H, 7.09; N, 19.70. Found: C, 50,47; H, 7.06; N, 19.62.

2-methylthio-4-dimethylamino-6-vinylpyrimidine (33a): White solid (130 mg, 70%). R_f[ethyl acetate/petroleum ether 1:6] = 0.58; mp = 44.7 °C; ^{1}H NMR (200 MHz, $CDCl_3$): δ = 6.52 (dd, J_{trans} = 17.33 Hz, J_{cis} = 10.04 Hz, 1H), 6.35 (dd, J_{trans} = 17.33 Hz, J_{gem} = 2.09 Hz, 1H), 6.01 (s, 1H), 5.47 (dd, J_{cis} = 10.04 Hz, J_{gem} = 2.09 Hz, 1H), 3.08 (s, 6H), 2.51 ppm (s, 3H); MS (ESI): m/z 196 $[M+H]^+$. Anal. for $C_9H_{13}N_3S$ Calcd: C, 55.35; H, 6.71; N, 21.52. Found: C, 55.12; H, 6.68; N, 21.43.

2-methylsulfonyl-4-dimethylamino-6-vinylpyrimidine (34a): White solid (60 mg, 57%). R_f[ethyl acetate/petroleum ether 1:1] = 0.34; mp = 260 °C (decomposition); IR ($CHCl_3$) $\tilde{\nu}$ = 1312, 1135 cm^{-1}; ^{1}H NMR (200 MHz, $CDCl_3$): δ = 6.57–6.46 (m, 2H), 6.34 (s, 1H), 5.58 (dd, J_{cis} = 9.82 Hz, J_{gem} = 1.85 Hz, 1H), 3.26 (s, 3H), 3.13 ppm (s, 6H). MS (ESI): m/z 228 $[M+H]^+$, 250 $[M+Na]^+$, 477 $[2M+Na]^+$. Anal. for $C_9H_{13}N_3O_2S$ Calcd: C, 47.56; H, 5.77; N, 18.49. Found: C, 47.36; H, 5.74; N, 18.41.

2-methylsulfonyl-4-dimethylamino-6-(2-hydroxyethyl)pyrimidine (35): Compound **32a** (1,0 g, 4,70 mmol) was dissolved in anhydrous CH_2Cl_2 (50 mL) and the resulting solution was cooled to 0 °C with an ice bath. A solution of 4-chloroperoxybenzoic acid (57–86%) (2,46 g, 9.39 mmol) in anhydrous CH_2Cl_2 (50 mL) was added dropwise. The reaction was stirred at room temperature for 4 h and then washed with $NaHCO_3$ (saturated solution; 80 mL). The aqueous phase was extracted with CH_2Cl_2 (5×80 mL). The organic extracts were collected, dried over anhydrous Na_2SO_4, and then evaporated under reduced pressure. The crude residue was purified by flash chromatography on silica gel column (eluent: CH_2Cl_2/CH_3OH 95:5 then 9:1) to give the desired product as a white solid (771 mg, 67%). R_f[CH_2Cl_2/CH_3OH 9:1] = 0.65; mp = 92.1–94.2 °C; IR ($CHCl_3$) $\tilde{\nu}$ = 3504, 1313, 1134 cm^{-1}; ^{1}H NMR (400 MHz, $CDCl_3$): δ = 6.38 (s, 1H), 3.83 (t, J = 5.72 Hz, 2H), 3.18 (s, 3H), 3.08 (s, 6H), 2.77 ppm (t, J = 5.72 Hz, 2H); ^{13}C NMR (400 MHz, $CDCl_3$): δ = 167.33, 164.47, 162.38, 103.67, 60.56, 39.79, 38.85, 37.37 ppm; MS (ESI): m/z 246 $[M+H]^+$, 268 $[M+Na]^+$, 513 $[2M+Na]^+$; Anal. for $C_9H_{15}N_3O_3S$ Calcd: C, 44.07; H, 6.16; N, 17.13. Found: C, 44.23; H, 6.18; N, 17.19.

2-methylamino-4-dimethylamino-6-(2-hydroxyethyl)pyrimidine (36): Compound **35** (50 mg, 0,20 mmol) dissolved in CH_3NH_2 (2.0 M solution in THF) (5,0 mL, 10,20 mmol) was irradiated in the microwave oven (sealed tube) for 30 min (3×10 min) at 130 °C. The solvent was evaporated under reduced pressure and the crude residue was purified by flash chromatography on silica gel column (eluent: CH_2Cl_2/CH_3OH 9:1) to give the desired product as white solid (31 mg, 78%). R_f[CH_2Cl_2/CH_3OH 9:1] = 0.25; mp = 70.4–71.6 °C; IR ($CHCl_3$) $\tilde{\nu}$ = 3460, 3316 cm^{-1}; ^{1}H NMR (200 MHz, $CDCl_3$): δ = 5.65 (s, 1H), 5.44 (bs, 2H), 3.86 (m, 2H), 3.01 (s, 6H), 2.87 (s, 3H), 2.64 ppm (m, 2H); MS (ESI): m/z 197 $[M+H]^+$; Anal. for $C_9H_{16}N_4O$ Calcd: C, 55.08; H, 8.22; N, 28.55. Found: C, 55.12; H, 8.25; N, 28.63.

2-methylamino-4-dimethylamino-6-vinylpyrimidine (37): Compound **36** (80 mg, 0,41 mmol) was dissolved in dry dioxane (7 mL). NaH (20 mg, 0,82 mmol) was added and the mixture was heated under reflux for 5 h. After cooling to RT, the residue was diluted with 20 mL of ice water and extracted with ethyl acetate (2× 20 mL). The organic phases were collected, dried over anhydrous Na_2SO_4, and evaporated under reduced pressure. The crude residue was purified by flash chromatography on silica gel column (eluent: CH_2Cl_2/CH_3OH 9:1) to give the desired product as colorless oil (30 mg, 41%). R_f[CH_2Cl_2/CH_3OH 9:1] = 0.60; IR ($CHCl_3$) $\tilde{\nu}$ = 3461 cm^{-1}; ^{1}H NMR (400 MHz, $CDCl_3$): δ = 6.46 (dd, J_{trans} = 17.29 Hz, J_{cis} = 10.46 Hz, 1H), 6.28 (d, J_{trans} = 17.29 Hz, 1H), 5.77 (s, 1H), 5.43 (d, J_{cis} = 10.46 Hz; 1H), 5.30 (bs, 1H), 3.06 (s, 6H), 2.95 ppm (s, 3H); ^{13}C NMR (200 MHz, CD_3OD): δ = 165.18, 163.12, 161.32, 136.79, 120.17, 91.66, 37.29, 28.37 ppm. MS (ESI): m/z 179 $[M+H]^+$ Anal. for $C_9H_{14}N_4$ Calcd: C, 60.65; H, 7.92; N, 31.43. Found: C, 60.74; H, 7.93; N, 31.48.

2-methylsulfonylamido-4-dimethylamino-6-(2-hydroxyethyl)pyrimidine (38): Compound **35** (50 mg, 0,20 mmol) was dissolved in

dry DMF (2 mL), then methanesulfonamide (388 mg, 4.08 mmol) and NaH (14 mg, 0.61 mmol) were added. The mixture was irradiated in the microwave oven (sealed tube) for 20 min (2×10 min) at 120 °C and then concentrated. After dilution with water, the mixture was neutralized with 1.0 M solution of HCl. The solvent was evaporated under reduced pressure and the crude residue was purified by flash chromatography on silica gel column (eluent: CH_2Cl_2/CH_3OH 9:1) to give the desired product as a white solid (29 mg, 54%). R_f[CH_2Cl_2/CH_3OH 9:1] = 0.37; mp = 173.9–175.1 °C; IR (nujol) $\tilde{\nu}$ = 3434, 3356, 1376, 1121 cm^{-1}; ^1H NMR (200 MHz, DMSO): δ = 11.42 (bs, 1H); 6.05 (s, 1H), 4.73 (t, J = 5.57 Hz, 1H); 3.68–3.59 (m, 2H), 3.07 (s, 6H), 2.96 (s, 3H), 2.54 ppm (t, J = 6.20 Hz, 2H); ^{13}C NMR (400 MHz, CD_3OD): δ = 162.66, 155.93, 155.64, 92.92, 59.32, 39.13, 36.73, 35.67 ppm. MS (ESI): m/z 261 $[M+H]^+$ 283 $[M+Na]^+$, 543 $[2M+Na]^+$. Anal. for $C_9H_{16}N_4O_3S$ Calcd: C, 41.53; H, 6.20; N, 21.52. Found: C, 41.57; H, 6.21; N, 21.59.

2-methylsulfonylamido-4-dimethylamino-6-vinylpyrimidine (39): Compound **38** (150 mg, 0,577 mmol) was dissolved in dry dioxane (30 mL), NaH (28 mg, 1,154 mmol) was added and the mixture was heated at reflux for 5 h. After cooling to RT, the residue was diluted with 35 mL of ice water and neutralized with 1.0 M solution of HCl. The aqueous phases were extracted with ethyl acetate (5×35 mL). The organic phases were collected, dried over anhydrous Na_2SO_4, and evaporated under reduced pressure. The crude residue was purified by flash chromatography on silica gel column (eluent: CH_2Cl_2/CH_3OH 95:5) to give the desired product as a white solid (58 mg, 42%). R_f[CH_2Cl_2/CH_3OH 95:5] = 0.42; mp = 183.6–185.3 °C; IR (nujol) $\tilde{\nu}$ = 1375, 1130 cm^{-1}; ^1H NMR (400 MHz, Acetone): δ = 9.32 (bs, 1H); 6.65 (dd, J_{trans} = 17.11 Hz, J_{cis} = 10.64 Hz, 1H), 6.40 (d, J_{trans} = 17.11 Hz, 1H), 6.36 (s, 1H); 5.55 (dd, J_{cis} = 10.64 Hz, 1H), 3.39 (s, 3H), 3.17 ppm (s, 6H); ^{13}C NMR (400 MHz, Acetone): δ = 163.65, 159.64, 156.80, 134.91, 120.17, 95.04, 40.89, 36.45 ppm; MS (ESI): m/z 243 $[M+H]^+$, 265 $[M+Na]^+$, 507 $[2M+Na]^+$; Anal. for $C_9H_{14}N_4O_2S$ Calcd: C, 44.61; H, 5.82; N, 23.12. Found: C, 44.70; H, 5.84; N, 23.19.

2-thiol-4-dimethylamino-6-(2-hydroxyethyl)pyrimidine (40): Compound **35** (350 mg, 1,43 mmol) was suspended in a 1 M aqueous solution of NaHS (12,3 mL). The reaction mixture was heated at reflux for 2 h and then the solvent was evaporated under reduced pressure. The crude residue was purified by flash chromatography on silica gel column (eluent: CH_2Cl_2/CH_3OH 9:1) to give the desired product as a white solid (182 mg, 64%). R_f[CH_2Cl_2/CH_3OH 9:1] = 0.46; mp = 260 °C (decomposition); IR (nujol) $\tilde{\nu}$ = 3328 cm^{-1}; ^1H NMR (400 MHz, CD_3OD): δ = 6.15 (s, 1H), 3.79 (t, J = 6.05 Hz, 2H), 3.21 (s, 3H), 3.08 (s, 3H), 2.67 ppm (t, J = 6.05 Hz, 2H); ^{13}C NMR (400 MHz, CD_3OD): δ = 178.44, 160.62, 154.79, 94.19, 59.26, 36.89, 36.37, 35.40 ppm; MS (ESI): m/z 200 $[M+H]^+$, 222 $[M+Na]^+$; Anal. for $C_8H_{13}N_3OS$ Calcd: C, 48.22; H, 6.58; N, 21.09. Found: C, 48.37; H, 6.60; N, 21.17.

General procedure for the synthesis of (41a and b): Compound **40** (1 mmol) was dissolved in anhydrous DMF (2 mL), then the opportune benzyl halide (*p*-methoxybenzyl chloride or *p*-cyanobenzyl bromide) (1.5 equiv mol^{-1}) and K_2CO_3 (1.3 equiv mol^{-1}) were added with stirring. The mixture was irradiated in the microwave oven (sealed tube) for 5 min at 130 °C, then the mixture was diluted with ethyl acetate (20 mL), and washed with water (2×40 mL). The organic phase was dried over anhydrous Na_2SO_4, the solvent was evaporated under reduced pressure. The crude residue was purified by flash chromatography on silica gel column (eluent: CH_2Cl_2/CH_3OH 95:5 for **41a** or ethyl acetate/petroleum ether 4:1 for **41b**) to give the desired product.

2-(4′-methoxybenzylthio)-4-dimethylamino-6-(2-hydroxyethyl)-pyrimidine (41a): Yellow oil (130 mg, 68%). R_f[CH_2Cl_2/CH_3OH 95:5] = 0.45; IR ($CHCl_3$) $\tilde{\nu}$ = 3394, 1588, 1512 cm^{-1}; ^1H NMR (200 MHz, $CDCl_3$): δ = 7.31 (d, J = 8.62 Hz, 2H), 6.81 (d, J = 8.62 Hz, 2H), 5.94 (s, 1H), 4.28 (s, 2H), 3.90 (t, J = 5.53 Hz, 2H), 3.76 (s, 3H), 3.06 (s, 6H), 2.73 ppm (t, J = 5.53 Hz, 2H); MS (ESI): m/z 320 $[M+H]^+$, 342 $[M+Na]^+$; Anal. for $C_{16}H_{21}N_3O_2S$ Calcd: C, 60.16; H, 6.63; N, 13.16. Found: C, 60.28; H, 6.65; N, 13.21.

2-(4′-cyanobenzylthio)-4-dimethylamino-6-(2-hydroxyethyl)pyrimidine (41b): White solid (390 mg, 82%). R_f[ethyl acetate/petroleum ether 4:1] = 0.26; mp = 122.0–124.2 °C. IR ($CHCl_3$) $\tilde{\nu}$ = 3389, 2230, 1591, 1508 cm^{-1}; ^1H NMR (200 MHz, $CDCl_3$): δ = 7.57–7.48 (m, 4H), 5.96 (s, 1H), 4.33 (s, 2H),3.88 (t, J = 5.49 Hz, 2H), 3.03 (s, 6H), 2.72 (t, J = 5.49 Hz, 2H); MS (ESI): m/z 315 $[M+H]^+$, 337 $[M+Na]^+$; Anal. for $C_{16}H_{18}N_4OS$ Calcd: C, 61.12; H, 5.77; N, 17.82. Found: C, 61.36; H,5.79; N, 17.89.

General procedure for the synthesis of of 42a and b: Compounds **41a** and **b** (1 mmol) were dissolved in dry dioxane (25 mL), NaH (2 equiv/mol) was added, and the mixture was heated under reflux for 3 h. After cooling to RT, the residue was diluted with 50 mL of ice water and extracted with ethyl acetate (2× 60 mL). The organic phases were collected, dried over anhydrous Na_2SO_4, and evaporated under reduced pressure. The crude residue was purified by flash chromatography on silica gel column (eluent: ethyl acetate-petroleum ether 1:2.5 for **42a**; 1:3 for **42b**) to give the desired product.

2-(4′-methoxybenzylthio)-4-dimethylamino-6-vinylpyrimidine (42a): Yellow oil (80 mg, 85%). R_f[ethyl acetate/petroleum ether 1:2.5] = 0.55; IR ($CHCl_3$) $\tilde{\nu}$ = 1583, 1510 cm^{-1}; ^1H NMR (200 MHz, $CDCl_3$): δ = 7.33 (d, J = 8.58 Hz, 2H), 6.80 (d, J = 8.58 Hz, 2H), 6.52 (dd, J_{trans} = 17.31 Hz, J_{cis} = 9.83 Hz, 1H), 6.37 (dd, J_{trans} = 17.31 Hz, J_{gem} = 2.15 Hz, 1H), 6.01 (s, 1H), 5.47 (dd, J_{cis} = 9.83 Hz, J_{gem} = 2.15 Hz, 1H), 4.35 (s, 2H), 3.75 (s, 3H), 3.06 ppm (s, 6H); MS (ESI): m/z 302 $[M+H]^+$, 324 $[M+Na]^+$; Anal. for $C_{16}H_{19}N_3OS$ Calcd: C, 63.76; H, 6.35; N, 13.94. Found: C, 63.52; H, 6.32; N, 13.89.

2-(4′-cyanobenzylthio)-4-dimethylamino-6-vinylpyrimidine (42b): White solid (180 mg, 95%). R_f[ethyl acetate/petroleum ether 1:3] = 0.54; mp = 92.7–94.4 °C; IR ($CHCl_3$) $\tilde{\nu}$ = 2228, 1583, 1506 cm^{-1}; ^1H NMR (200 MHz, $CDCl_3$): 7.53 (s, 4H), 6.51 (dd, J_{trans} = 17.33 Hz, J_{cis} = 10.49 Hz, 1H), 6.33 (dd, J_{trans} = 17.33 Hz, J_{gem} = 1.95 Hz, 1H), 6.02 (s, 1H), 5.48 (dd, J_{cis} = 10.49 Hz, J_{gem} = 1.95 Hz, 1H), 4.39 (s, 2H), 3.04 ppm (s, 6H); MS (ESI): m/z 297 $[M+H]^+$; Anal. for $C_{16}H_{18}N_4S$ Calcd: C, 64.40; H, 6.08; N, 18.78. Found: C, 64.65; H, 6.10; N, 18.85.

General procedure for the synthesis of 43a and b: Compounds **42a** and **b** (1 mmol) were dissolved in CH_3OH (20 mL) (for **42a**, 2 mL of CH_2Cl_2 was also added). A water solution (20 mL) of OXONE (3 equiv/mol) was added dropwise and the resulting mixture stirred at RT overnight. The crude residue was concentrated under reduced pressure and extracted with ethyl acetate (3× 50 mL). The organic phases were collected, dried over anhydrous Na_2SO_4, and evaporated under reduced pressure. The crude residue was purified by flash chromatography on silica gel column (eluent: ethyl acetate-petroleum ether 2:1) to give the desired product.

2-(4′-methoxybenzylsulfonyl)-4-dimethylamino-6-vinylpyrimidine (43a): White solid (40 mg, 56%). R_f [ethyl acetate/petroleum ether 2:1] = 0.63; mp = 260 °C (decomposition); IR ($CHCl_3$) $\tilde{\nu}$ = 1597, 1513, 1313, 1122 cm^{-1}; ^1H NMR (200 MHz, $CDCl_3$): δ = 7.33 (d, J = 8.64 Hz, 2H), 6.83 (d, J = 8.64 Hz, 2H), 6.62 (dd, J_{trans} = 17.39 Hz, J_{cis} = 9.77 Hz, 1H), 6.48 (dd, J_{trans} = 17.39 Hz, J_{gem} = 2.06 Hz, 1H), 6.33

(s,1H), 5.62 (dd, J_{cis} = 9.77 Hz, J_{gem} = 2.06 Hz, 1H), 4.70 (s, 2H), 3.75 (s, 3H), 3.14 ppm (s, 6H); MS (ESI): *m/z* 334 $[M+H]^+$, 356 $[M+Na]^+$, 372 $[M+K]^+$, 689 $[2M+Na]^+$, 705 $[2M+K]^+$. Anal. for $C_{16}H_{19}N_3O_3S$ Calcd: C, 57.64; H, 5.74; N, 12.60. Found: C, 57.81; H, 5.76; N, 12.65.

2-(4′-cyanobenzylsulfonyl)-4-dimethylamino-6-vinylpyrimidine (43b): White solid (90 mg, 58%). R_f[ethyl acetate/petroleum ether 2:1] = 0.57; mp = 195.1–197.0 °C; IR ($CHCl_3$) $\tilde{\nu}$ = 1597, 1498, 2232, 1323, 1125 cm^{-1}; ^1H NMR (400 MHz, $CDCl_3$): δ = 7.62–7.52 (m, 4H), 6.62 (dd, J_{trans} = 17.20 Hz, J_{cis} = 10.40 Hz, 1H), 6.47 (d, J_{trans} = 17.20 Hz, 1H), 6.39 (s, 1H), 5.65 (d, J_{cis} = 10.40 Hz, 1H), 4.81 (s, 2H), 3.16 ppm (s, 6H); MS (ESI): *m/z* 329 $[M+H]^+$, 351 $[M+Na]^+$, 367 $[M+K]^+$, 679 $[2M+Na]^+$; Anal. for $C_{16}H_{16}N_4O_2S$ Calcd: C, 58.52; H, 4.91; N, 17.06. Found: C, 58.75; H, 4.92; N, 17.12.

General procedure for the synthesis of compounds 46a–c: Compounds **45a–c** (1 mmol) were dissolved in absolute ethanol (15 mL), then K_2CO_3 (1.1 equiv/mol), and dimethylamine (2 M solution in THF; 1.5 equiv/mol) were added. The mixture was heated under reflux for 1 h and then the solvent was evaporated under reduced pressure. The crude residue was purified by flash chromatography on silica gel column (eluent: ethyl acetate-petroleum ether 1:1 for **46a–b** and 1:2 for **46c**) to give the desired product.

2-Methylthio-4-dimethylamino-5-chloro-6-(2-hydroxyethyl)-pyrimidine (46a): White solid (145 mg, 73%). R_f [ethyl acetate/petroleum ether 1:1] = 0.66; mp = 75.2–76.9 °C: IR ($CHCl_3$) $\tilde{\nu}$ = 3436 cm^{-1}; ^1H NMR (200 MHz, $CDCl_3$): δ = 3.97 (t, *J* = 5.72 Hz, 2H), 3.21 (s, 6H), 3.03 (t, *J* = 5.72 Hz, 2H), 2.48 ppm (s, 3H); MS (ESI): *m/z* 248 $[M+H]^+$, 270 $[M+Na]^+$, 286 $[M+K]^+$; Anal. for $C_9H_{14}ClN_3OS$ Calcd: C, 43.63; H, 5.70; N, 16.96. Found: C, 43.45; H, 5.67; N, 16.89.

2-Methylthio-4-dimethylamino-5-bromo-6-(2-hydroxyethyl)-pyrimidine (46b): White solid (199 mg, 95%). R_f[ethyl acetate/petroleum ether 1:1] = 0.67; mp = 61.2–62.1 °C; IR ($CHCl_3$) $\tilde{\nu}$ = 3436 cm^{-1}; ^1H NMR (200 MHz, $CDCl_3$): δ = 3.97 (t, *J* = 5.39 Hz, 2H), 3.15 (s, 6H), 2.98 (t, *J* = 5.39 Hz, 2H), 2.46 ppm (s, 3H); MS (ESI): *m/z* 293 $[M+H]^+$, 315 $[M+Na]^+$; Anal. for $C_9H_{14}BrN_3OS$ Calcd: C, 36.99; H, 4.83; N, 14.38. Found: C, 37.10; H, 4.84; N, 14.42.

2-Methylthio-4-dimethylamino-5-iodo-6-(2-hydroxyethyl)-pyrimidine (46c): Yellow oil (168 mg, 77%). R_f[ethyl acetate/petroleum ether 1:2] = 0.67; IR ($CHCl_3$) $\tilde{\nu}$ = 3439 cm^{-1}; ^1H NMR (200 MHz, $CDCl_3$): 3.93 (t, *J* = 5.21 Hz, 2H), 3.09 (s, 6H), 2.97 (t, *J* = 5.21 Hz, 2H), 2.45 ppm (s, 3H); MS (ESI): *m/z* 340 $[M+H]^+$, 362 $[M+Na]^+$, 378 $[M+K]^+$; Anal. for $C_9H_{14}IN_3OS$ Calcd: C, 31.87; H, 4.16; N, 12.39. Found: C, 31.74; H, 4.14; N, 12.34.

General procedure for the synthesis of compounds 47a–c: Compounds **46a–c** (1 mmol) were dissolved in dry dioxane (25 mL), NaH (2 equiv/mol) was added, and the mixture was heated under reflux for 3 h. After cooling to RT, the residue was diluted with 50 mL of ice water and extracted with ethyl acetate (2×50 mL). The organic phases were collected, dried over anhydrous Na_2SO_4, and evaporated under reduced pressure. The crude product was purified by flash chromatography on silica gel column (eluent: ethyl acetate-petroleum ether 5:95 for **47a–b** and 3:97 for **47c**) to give the desired product.

2-Methylthio-4-dimethylamino-5-chloro-6-vinylpyrimidine (47a): White solid (105 mg, 78%). R_f[ethyl acetate/petroleum ether 5:95] = 0.64; mp = 56.1–57.4 °C; ^1H NMR (200 MHz, $CDCl_3$): δ = 7.13 (dd, J_{trans} = 17.09 Hz, J_{cis} = 10.03 Hz, 1H), 6.56 (dd, J_{trans} = 17.09 Hz, J_{gem} = 1.99 Hz, 1H), 5.61 (dd, J_{cis} = 10.03 Hz, J_{gem} = 1.99 Hz, 1H), 3.15 (s, 6H), 2.50 ppm (s, 3H); MS (ESI): *m/z* 230 $[M+H]^+$; Anal. for $C_9H_{12}ClN_3S$ Calcd: C, 47.05; H,5.27; N, 18.29. Found: C, 46.86; H, 5.24; N, 18.21.

2-Methylthio-4-dimethylamino-5-bromo-6-vinylpyrimidine (47b): White solid (131 mg, 70%). R_f[ethyl acetate/petroleum ether 5:95] = 0.65; mp = 49.8–51.0 °C; ^1H NMR (200 MHz, $CDCl_3$): δ = 7.13 (dd, J_{trans} = 16.70 Hz, J_{cis} = 10.75 Hz, 1H), 6.54 (dd, J_{trans} = 16.70 Hz, J_{gem} = 2.00 Hz, 1H), 5.56 (dd, J_{cis} = 10.75 Hz, J_{gem} = 2.00 Hz, 1H), 3.12 (s, 6H), 2.50 ppm (s, 3H); MS (ESI): *m/z* 275 $[M+H]^+$; Anal. for $C_9H_{12}BrN_3S$ Calcd: C, 39.43; H,4.41; N, 15.33. Found: C, 39.55; H, 4.42; N, 15.38.

2-Methylthio-4-dimethylamino-5-iodo-6-vinylpyrimidine (47c): Yellow solid (140 mg, 88%). R_f [ethyl acetate/petroleum ether 3:97] = 0.51; mp = 55.9–57.3 °C; ^1H NMR (200 MHz, $CDCl_3$): δ = 7.08 (dd, J_{trans} = 16.37 Hz, J_{cis} = 10.03 Hz, 1H), 6.49 (dd, J_{trans} = 16.37 Hz, J_{gem} = 1.98 Hz, 1H), 5.53 (dd, J_{cis} = 10.03 Hz, J_{gem} = 1.98 Hz, 1H), 3.09 (s, 6H), 2.51 ppm (s, 3H); MS (ESI): *m/z* 322 $[M+H]^+$, 344 $[M+Na]^+$, 360 $[M+K]^+$; Anal. for $C_9H_{12}IN_3S$ Calcd: C, 33.66; H, 3.77; N, 13.06. Found: C, 33.79; H, 3.78; N, 13.11.

General procedure for the synthesis of compounds 48a–c: Compounds **47a–c** (1 mmol) were dissolved in a mixture of CH_3OH/CH_2Cl_2 10:3 (13 mL). A water solution (13 mL) of OXONE® (3 equiv/mol) was added dropwise and the mixture stirred at RT overnight. The crude residue was concentrated under reduced pressure and extracted with ethyl acetate (3×13 mL). The organic phases were collected, dried over anhydrous Na_2SO_4, and evaporated under reduced pressure. The crude residue was purified by flash chromatography on silica gel column (eluent: ethyl acetate-petroleum ether 1:1 for **48a–b** and 1:2 for **48c**) to give the desired product.

2-Methylsulfonyl-4-dimethylamino-5-chloro-6-vinylpyrimidine (48a): White solid (69 mg, 80%). R_f[ethyl acetate/petroleum ether 1:1] = 0.59; mp = 260 °C (decomposition); IR ($CHCl_3$) $\tilde{\nu}$ = 1314, 1137 cm^{-1}; ^1H NMR (200 MHz, $CDCl_3$): δ = 7.15–7.09 (m, 1H), 6.65 (d, J_{trans} = 16.77 Hz, 1H), 5.75 (d, J_{cis} = 10.58 Hz, 1H), 3.28 (s, 3H), 3.13 ppm (s, 6H); MS (ESI): *m/z* 262 $[M+H]^+$, 284 $[M+Na]^+$, 545 $[2M+Na]^+$; Anal. for $C_9H_{12}ClN_3O_2S$ Calcd: C, 41.30; H, 4.62; N, 16.05. Found: C, 41,13; H, 4,60; N, 15.98.

2-Methylsulfonyl-4-dimethylamino-5-bromo-6-vinylpyrimidine (48b): White solid (77 mg, 41%). R_f[ethyl acetate/petroleum ether 1:1] = 0.61; mp = 111.2–112.0 °C; IR ($CHCl_3$) $\tilde{\nu}$ = 1316, 1138 cm^{-1}; ^1H NMR (200 MHz, $CDCl_3$): δ = 7.21 (dd, J_{trans} = 16.65 Hz, J_{cis} = 10.83 Hz, 1H), 6.64 (d, J_{trans} = 16.65 Hz, 1H), 5.74 (dd, J_{cis} = 10.83 Hz, J_{gem} = 1.90 Hz, 1H), 3.29 (s, 3H), 3.26 ppm (s, 6H); MS (ESI): *m/z* 307 $[M+H]^+$, 329 $[M+Na]^+$, 635 $[2M+Na]^+$; Anal. for $C_9H_{12}BrN_3O_2S$ Calcd: C, 35.30; H, 3.95; N, 13.72. Found: C, 35.41; H, 3.96; N, 13.75.

2-Methylsulfonyl-4-dimethylamino-5-iodo-6-vinylpyrimidine (48c): Yellow oil (92 mg, 60%). R_f [ethyl acetate/petroleum ether 1:2] = 0.46; IR ($CHCl_3$) $\tilde{\nu}$ = 1315, 1138 cm^{-1}; ^1H NMR (200 MHz, $CDCl_3$): δ = 7.14 (dd, J_{trans} = 16.65 Hz, J_{cis} = 9.89 Hz, 1H), 6.60 (d, J_{trans} = 16.65 Hz, 1H), 5.68 (d, J_{cis} = 9.89 Hz, 1H), 3.29 (s, 3H), 3.24 ppm (s, 6H); MS (ESI): *m/z* 354 $[M+H]^+$, 376 $[M+Na]^+$, 729 $[2M+Na]^+$; Anal. for $C_9H_{12}IN_3O_2S$ Calcd: C, 30.61; H, 3.42; N, 11.90. Found: C, 30.73; H, 3.43; N, 11.94.

Acknowledgements

This study was supported by grants from the European TRIoH Consortium (EU Contract LSHBCT-2003-503480-TRIoH).

Keywords: 3,4-dihydro-2-alkoxy-6-benzyl-4-oxypyrimidines (DABOs) · HIV-1 · lead discovery · non-nucleoside reverse transcriptase inhibitors (NNRTIs) · reverse transcriptase (RT)

[1] http://www.unaids.org/en/HIV_data/2006GlobalReport/default.asp.
[2] G. Barbaro, G. Barbini, *Chemotherapy* **2006**, *52*, 161–165.
[3] a) L. R. Boone, *Curr. Opin. Invest. Drugs* **2006**, *7*, 128–135.; b) G. Barbaro, A. Scozzafava, A. Mastrolorenzo, C. T. Supuran, *Curr. Pharm. Des.* **2005**, *11*, 1805–1843.
[4] M. Botta, M. Artico, S. Massa, A. Gambacorta, M. E. Marongiu, A. Pani, P. La Colla, *Eur. J. Med. Chem.* **1992**, *27*, 251–257.
[5] M. Artico, *Drug. Future* **2002**, *27*, 159–175.
[6] D. M. Himmel, K. Das, A. D. Clark, Jr., S. H. Hughes, A. Benjahad, S. Oumouch, J. Guillemont, S. Coupa, A. Poncelet, I. Csoka, C. Meyer, K. Andries, C. H. Nguyen, D. S. Grierson, E. Arnold, *J. Med. Chem.* **2005**, *48*, 7582–7591.
[7] A. L. Hopkins, J. Ren, R. M. Esnouf, B. E. Willcox, E. Y. Jones, C. Ross, T. Miyasaka, R. T. Walker, H. Tanaka, D. K. Stammers, D. I. Stuart, *J. Med. Chem.* **1996**, *39*, 1589–1600.
[8] J. Ren, R. Esnouf, A. Hopkins, C. Ross, Y. Jones, D. Stammers, D. Stuart, *Structure* **1995**, *3*, 915–926.
[9] J. Ding, K. Das, H. Moereels, L. Koymans, K. Andries, P. A. J. Janssen, S. H. Hughes. E. Arnold, *Nat. Struct. Biol.* **1995**, *2*, 407–415.
[10] Y. Hsiou, J. Ding, K. Das, A. D. Clark, Jr., S. H. Hughes, E. Arnold, *Structure* **1996**, *4*, 853–860.
[11] R. Esnouf, J. Ren, C. Ross, Y. Jones, D. Stammers, D. Stuart, *Nat. Struct. Biol.* **1995**, *2*, 303–308.
[12] P. P. Mager, *Drug Des. Discovery* **1996**, *14*, 241–257.
[13] K. Dasa, P. J. Lewib, S. H. Hughesc, E. Arnold, *Prog. Biophys. Mol. Biol.* **2005**, *88*, 209–231.
[14] R. F. Schinazi, B. A. Larder, J. W. Mellors, *Int. J. Surg. Pathol. Int. AntiVir. News* **2000**, *8*, 65–91.
[15] G. Maga, M. Amacker, N. Ruel, U. Hübscher, S. Spadari, *J. Mol. Biol.* **1997**, *274*, 738–747.
[16] Y. Hsiou, J. Ding, K. Das, A. D. Clark, Jr., P. L. Boyer, P. Lewi, P. A. J. Janssen, J. P. Kleim, M. Rösner, S. H. Hughes, E. Arnold, *J. Mol. Biol.* **2001**, *309*, 437–445.
[17] F. Manetti, J. A. Esté, I. Clotet-Codina, M. Armand-Ugon, G. Maga, E. Crespan, R. Cancio, C. Mugnaini, C. Bernardini, A. Togninelli, C. Carmi, M. Alongi, E. Petricci, S. Massa, F. Corelli, M. Botta, *J. Med. Chem.* **2005**, *48*, 8000–8008.
[18] M. Botta, F. Occhionero, R. Nicoletti, P. Mastromarino, C. Conti, M. Magrini, R. Saladino, *Bioorg. Med. Chem.* **1999**, *7*, 1925–1931.
[19] Three-dimensional coordinates of the HIV-1 RT/TNK561 complex (Brookhaven Protein Data Bank entry 1RT2) were used as the input structure for docking calculations.
[20] R. J. Clay, T. A. Collom, G. L. Karrick, J. A. Wemple, *Synthesis* **1993**, 290–292.
[21] M. Radi, L. Contemori, D. Castagnolo, R. Spinosa, J. A. Esté, S. Massa, M. Botta, *Org. Lett.* **2007**, *9*, 3157–3160.
[22] Data not shown.
[23] M. Radi, E. Petricci, G. Maga, F. Corelli, M. Botta, *J. Comb. Chem.* **2005**, *7*, 117–122.
[24] a) K. S. Webb, *Tetrahedron Lett.* **1994**, *35*, 3457–3460; b) B. M. Trost, D. P. Curran, *Tetrahedron Lett.* **1981**, *22*, 1287–1290.
[25] C. Mugnaini, E. Petricci, M. Botta, F. Corelli, P. Mastromarino, G. Giorni, *Eur. J. Med. Chem.* **2007**, *42*, 256–262.
[26] TNK-651 was synthesized following a literature procedure; physical and spectroscopic data were consistent with those reported: A. L. Hopkins, J. Ren, R. M. Esnouf, B. E. Willcox, E. Y. Jones, C. Ross, T. Miyasaka, R. T. Walker, H. Tanaka, D. K. Stammers, D. I. Stuart, *J. Med. Chem.* **1996**, *39*, 1589–1600.
[27] G. Maga, M. Radi, S. Zanoli, F. Manetti, R. Cancio, U. Hübscher, S. Spadari, C. Falciani, M. Terrazas, J. Vilarrasa, M. Botta, *Angew. Chem.* **2007**, *119*, 1842–1845; *Angew. Chem. Int. Ed.* **2007**, *46*, 1810–1813.
[28] R. A. Spence, W. M. Kati, K. S. Anderson, K. A. Johnson, *Science.* **1995**, *267*, 988–993.
[29] R. A. Spence, K. S. Anderson, K. A. Johnson, *Biochemistry* **1996**, *35*, 1054–1063.
[30] Data not shown.
[31] J. Balzarini, A. Karlsson, M. J. Perez-Perez, L. Vrang, J. Walbers, H. Zhang, B. Öberg, A. M. Vandamme, M. J. Camarasa, E. De Clercq, *Virology* **1993**, *192*, 246–253.
[32] J. W. Mellors, G. E. Dutschman, G. J. Im, E. Tramontano, S. R. Winkler, Y. C. Cheng, *Mol. Pharmacol.* **1992**, *41*, 446–451.
[33] J. H. Nunberg, W. A. Schleif, E. J. Boots, J. A. O'Brien, J. C. Quintero, J. M. Hoffman, E. A. Emini, M. E. Goldman, *J. Virol.* **1991**, *65*, 4887–4892.
[34] Data not shown.
[35] J. Lindberg, S. Sigurdsson, S. Lowgren, H. O. Andersson, C. Sahlberg, R. Noreen, K. Fridborg, H. Zhang, T. Unge, *Eur. J. Biochem.* **2002**, *269*, 1670–1677.
[36] Z. Zhou, M. Madrid, J. D. Madura, *Proteins Struct. Funct. Genet.* **2002**, *49*, 529–542.
[37] P. H. Patel, A. J. Molina, J. Ding, C. Tantillo, A. D. Clark, Jr., R. Raag, R. G. Nanni, S. H. Hughes, E. Amold, *Biochemistry* **1995**, *34*, 5351–5363.
[38] P. L. Boyer, A. L. Ferris, S. H. Hughes, *J. Virol.* **1992**, *66*, 1031–1039.
[39] J. Wang, S. J. Smerdon, J. Jager, L. A. Kohlstaedt, P. A. Rice, J. M. Friedman, T. A. Steitz, *Proc. Natl. Acad. Sci. USA* **1994**, *91*, 7242–7246.
[40] K. Das, A. D. Clark Jr. , P. J. Lewi, J. Heeres, M. R. De Jonge, L. M. Koymans, H. M. Vinkers, F. Daeyaert, D. W. Ludovici, M. J. Kukla, B. De Corte, R. W. Kavash, C. Y. Ho, H. Ye, M. A. Lichtenstein, K. Andries, R. Pauwles, M. P. Debethune, P. L. Boyer, P. Clark, S. H. Hughes, P. A. Janssen, E. Arnold, *J. Med. Chem.* **2004**, *47*, 2550–2560.
[41] D. W. Rodgers, S. J. Gamblin, B. A. Harris, S. Ray, J. S. Culp, B. Hellmig, D. J. Woolf, C. Debouck, S. C. Harrison, *Proc. Natl. Acad. Sci. USA* **1995**, *92*, 1222–1226.
[42] J. Ren, R. Esnouf, E. Garman, D. Somers, C. Ross, I. Kirby, J. Keeling, G. Darby, Y. Jones, D. Stuart, D. Stammers, *Nat. Struct. Biol.* **1995**, *2*, 293–302.
[43] M. E. Goldman, J. H. Nunberg, J. A. O'Brien, J. C. Quintero, W. A. Schleif, K. F. Freund, S. L. Gaul, W. S. Saari, J. S. Wai, J. M. Hoffman, P. S. Anderson, D. J. Hupe, E. A. Emini, A. M. Stern, *Proc. Natl. Acad. Sci. USA* **1991**, *88*, 6863–6867.
[44] The PyMOL Molecular Graphics System, DeLano Scientific, San Carlos, CA (USA): W. L. DeLano, *Biotechnol.* **2002**, *58*, 721–727.
[45] F. Mohamadi, N. G. J. Richards, W. C. Guida, R. Liskamp, M. Lipton, C. Caufield, G. Chang, T. Hendrickson, W. C. Still, *J. Comput. Chem.* **1990**, *11*, 440–467.
[46] Maestro version 6.0 is distributed by Schrödinger.

Received: August 3, 2007
Revised: September 5, 2007
Published online on December 14, 2007

